

Award Number: W81XWH-05-C-0004

TITLE: Targeted Therapies for Myeloma and Metastatic Bone Cancers

PRINCIPAL INVESTIGATOR: Neal Vail, Ph.D.

CONTRACTING ORGANIZATION: Southwest Research Institute  
San Antonio TX 78238

REPORT DATE: February 2007

TYPE OF REPORT: Annual

PREPARED FOR: U.S. Army Medical Research and Materiel Command  
Fort Detrick, Maryland 21702-5012

DISTRIBUTION STATEMENT: Approved for Public Release;  
Distribution Unlimited

The views, opinions and/or findings contained in this report are those of the author(s) and should not be construed as an official Department of the Army position, policy or decision unless so designated by other documentation.

# REPORT DOCUMENTATION PAGE

*Form Approved*  
*OMB No. 0704-0188*

Public reporting burden for this collection of information is estimated to average 1 hour per response, including the time for reviewing instructions, searching existing data sources, gathering and maintaining the data needed, and completing and reviewing this collection of information. Send comments regarding this burden estimate or any other aspect of this collection of information, including suggestions for reducing this burden to Department of Defense, Washington Headquarters Services, Directorate for Information Operations and Reports (0704-0188), 1215 Jefferson Davis Highway, Suite 1204, Arlington, VA 22202-4302. Respondents should be aware that notwithstanding any other provision of law, no person shall be subject to any penalty for failing to comply with a collection of information if it does not display a currently valid OMB control number. **PLEASE DO NOT RETURN YOUR FORM TO THE ABOVE ADDRESS.**

<b>1. REPORT DATE</b> 01-02-2007			<b>2. REPORT TYPE</b> Annual		<b>3. DATES COVERED</b> 18 Jan 2006 – 17 Jan 2007	
<b>4. TITLE AND SUBTITLE</b>  Targeted Therapies for Myeloma and Metastatic Bone Cancers					<b>5a. CONTRACT NUMBER</b>	
					<b>5b. GRANT NUMBER</b> W81XWH-05-C-0004	
					<b>5c. PROGRAM ELEMENT NUMBER</b>	
<b>6. AUTHOR(S)</b>  Neal Vail, Ph.D.  Email: nveil@swri.org					<b>5d. PROJECT NUMBER</b>	
					<b>5e. TASK NUMBER</b>	
					<b>5f. WORK UNIT NUMBER</b>	
<b>7. PERFORMING ORGANIZATION NAME(S) AND ADDRESS(ES)</b>  Southwest Research Institute San Antonio TX 78238					<b>8. PERFORMING ORGANIZATION REPORT NUMBER</b>	
<b>10. SPONSOR/MONITOR'S ACRONYM(S)</b>					<b>11. SPONSOR/MONITOR'S REPORT NUMBER(S)</b>	
<b>13. SUPPLEMENTARY NOTES</b> Original contains colored plates: ALL DTIC reproductions will be in black and white.						
<b>14. ABSTRACT</b>  Developed two procedures for preparing nanoparticles and demonstrated their ability to repeatedly produce nanoparticles with narrow distribution in the target particle size range of 70-200nm and smaller, if necessary. Synthesized and fully characterized PLA-b-PEG-Maleimide block copolymers to facilitate the attachment of bone-targeting ligands to polymer nanoparticles via thiol coupling. Improved lyostability of polymer nanoparticles, with and without PEG modification. Developed methods to radiolabel polymer nanoparticles, the first time, to our knowledge, this has been done. Encapsulated two proteasome inhibitors, MG-132 and PS-1, and determined their in vitro release profiles. Developed proteasome activity assay to determine activity of encapsulated drug. Developing in vitro assay to determine affinity of bone-targeting nanoparticles to hydroxyapatite substrates.						
<b>15. SUBJECT TERMS</b> Bone Cancer therapy						
<b>16. SECURITY CLASSIFICATION OF:</b>				<b>17. LIMITATION OF ABSTRACT</b>	<b>18. NUMBER OF PAGES</b>	<b>19a. NAME OF RESPONSIBLE PERSON</b> USAMRMC
<b>a. REPORT</b> U	<b>b. ABSTRACT</b> U	<b>c. THIS PAGE</b> U	<b>19b. TELEPHONE NUMBER</b> (include area code)			

## Table of Contents

Introduction.....	4
Body.....	4
Key Research Accomplishments .....	9
Reportable Outcomes.....	9
Conclusions.....	9
References.....	9
Appendix 1. Figures.....	10
Appendix 2. NMR Report.....	13
Appendix 3. Abstracts.....	31

## Introduction

The goal of this project is to determine, in preclinical studies, the potential of skeletally targeted proteasome inhibitors as an efficacious and selective treatment for myeloma. We have found that several proteasome inhibitors are effective against both human and murine myeloma cells in culture. However, as with any proteasome inhibitor, there are serious concerns over the potential systemic effects and toxicity. Our hypothesis is that bone-targeting nanocarriers can preferentially accumulate in the skeleton and locally release proteasome inhibitors to impair the capacity of myeloma cells to survive and grow in vivo, thereby reducing the formation and growth of tumor-induced lytic bone lesions. Proteasome inhibitors are otherwise not selective to bone and their therapeutic-toxic window may be narrow when administered systemically. The scope of this project is to validate our hypothesis. The major tasks are: 1. Formulate and characterize drug-containing, bone-targeting nanocapsules; 2. Determine the in vivo biodistribution of bone-targeting nanocapsules; and, 3. Evaluate the efficacy of bone-targeted delivery of proteasome inhibitors on myeloma tumor progression using the 5TGM1 murine model of myeloma. The outcomes of this research will be significant. The study will demonstrate the preferential biodistribution of nanocarriers specifically designed to target and adhere to bone matrices. It will further show that these same nanocapsules can selectively deliver a specific and potent proteasome inhibitor to skeletal sites to act as an anti-myeloma agent. Targeted bone delivery has several potential benefits, including reduced systemic exposure, increased efficacy in the targeted microenvironment, and the ultimate opportunity to reverse catastrophic disease processes. Furthermore, targeted delivery to bone has several additional significant application opportunities in the areas of osteoporosis, fracture healing, cartilage repair, and tissue engineering.

## Body

The project is broken down into the following tasks:

1. Formulate and characterize drug-containing, bone-targeting nanocarriers
2. Determine the in vivo biodistribution of bone-targeting nanocarriers
3. Demonstrate the efficacy of bone-targeted delivery of proteasome inhibitors on myeloma tumor progress

Task 1 was scheduled to occur during years 1 – 2 of the project, Task 2 during years 2 – 3 of the project with some overlap with Task 1, and Task 3 is scheduled to occur during the last year and one-half of the project. Therefore, in this second annual report, there are no technical accomplishments to be reported for Task 3.

Task 1 is focused on the development of the bone-targeting nanoparticles and is broken down into the following subtasks:

1. Selection of proteasome inhibitors for in vivo studies – Completed and reported in first annual report.
2. Formulation and characterization of bone-targeting nanoparticles – Discussed in first annual report and further discussed in this annual report.
3. Demonstration of adhesion of bone-targeting nanoparticles to bone-like substrates in vitro – Discussed in this annual report.
4. Formulation of proteasome inhibitors into bone-targeting nanoparticles – Discussed in this annual report.

The bulk of the work during this year of the project was focused on further development and characterization of bone-targeting nanoparticles. This consisted of the following tasks:

1. Lyoprotection of nanoparticles.
2. Fluorescent labeling of nanoparticles.
3. Synthesis of functionalized block copolymers for attaching bone-targeting ligands
4. Radiolabeling of nanoparticles
5. Encapsulation of proteasome inhibitors
6. Attachment of bone-targeting ligands to nanoparticles

In the first year of the project, we developed standard protocols for preparing nanoparticles from combinations of polylactide-co-glycolide (PLGA) and PLGA-b-mPEG polymers. The synthesis of the later materials was also developed during the first year of the project. We developed two protocols for preparing narrowly-distributed nanoparticles in the size range of about 100-200nm: an emulsion/solvent evaporation technique and nanoprecipitation. Both methods are robust and yield reproducible results. The emulsion/solvent evaporation method tends to yield larger particles than the nanoprecipitation method. The difference in the two methods lies in the miscibility of the polymer solvent with the continuous aqueous phase. In precipitation the solvent is completely miscible with water. The emulsification method is suitable for encapsulating either hydrophilic or lipophilic drugs, while the precipitation method is suitable only for lipophilic drugs. In both methods, the particle size can be effectively tuned by altering the polymer concentration in the initial organic phase. We found cross-flow filtration to be an effective means of removing both low- and high-boiling solvents, and integrated this method into our nanoparticle preparation protocols. We further found it necessary to concentrate the resulting nanoparticles using centrifuge concentrator tubes and we have integrated this processing step into our nanoparticle preparation protocol.

In the last annual report, we discussed the lyoprotection of nanoparticle preparations using various low molecular weight sugars. Lyoprotection is important to produce storage-stable nanoparticles in dry form, allowing us to prepare large, single batches of material that can be fully characterized, stored, and used as needed for upcoming animal

studies. While selected sugars showed some lyostability, stability could only be achieved with high sugar levels, typically on the order of 25% wt. or more of the total nanoparticle dispersion volume. We had concerns for this high sugar content in actual in vivo applications. Therefore, we examined alternative means of lyoprotection. We found anecdotal evidence that polyvinylpyrrolidone (PVP) and polaxomers (nonionic, ethylene oxide/propylene oxide block copolymers) have cryoprotection capacity. Pluronic F68 was selected for study based on availability. F68 is a difunctional block copolymer surfactant terminating in primary hydroxyl groups. It is a nonionic surfactant that is 100% active and considered generally recognized as safe (GRAS). We found this material to provide excellent lyostability at extremely low concentrations compared to previous work with sugars (see Figure 1). The addition of 100x of F68 relative to the amount of PLGA-mPEG block copolymer in nanoparticles comprised of a mixture of PLGA:PLGA-mPEG (w/w 90/10) resulted in redispersible, non-agglomerated nanoparticles. In this case, the amount of lyoprotectant necessary to achieve lyostability is on the order of about 1% wt. of the total nanoparticle dispersion, significantly lower than the quantities required when using sugars. We have since incorporated this lyoprotection method into our nanoparticle formulation protocols.

We were interested in fluorescently labeling our nanoparticles to aid in their quantification in other characterization assays. The preferred approach was to encapsulate a fluorescent agent in the nanoparticles. We first considered quantum dots (QD) because of their high quantum yield and selectable fluorescent wavelengths. We initially reported success in encapsulating two QD systems with emission wavelengths of 520nm (green) and 620nm (red). However, on closer examination of the results, we found that QDs were not encapsulated into the particles and subsequent work demonstrated that it was not possible to encapsulate QD particles without compromising the colloidal stability of the resulting nanoparticles. Therefore, we abandoned the encapsulation of QDs as fluorescent markers. Subsequently, we studied and developed fluorescent nanoparticles incorporating small molecule organic dyes, such as rhodamine B and others.

In the last annual report, we discussed the difficulties encountered with preparing a functionalized polymer to support the attachment of selected bone-targeting ligands. Shortly before the report was submitted, we confirmed the preparation of a PLG-b-PEG-maleimide material discussed in the original proposal (Task 1.2, Proposal Section 5.2). Preliminary characterization of this material by simple NMR techniques confirmed the synthesis, but also indicated a low yield of the product. After consulting with our NMR spectroscopist, we conducted a more thorough analysis of the synthesized materials at various points in the synthetic approach and determined the product was produced in quantitative yield. This detailed NMR analysis is summarized in an internal report provided in the Appendix. We have since prepared stock quantities of this material.

We developed methods of radiolabeling nanoparticles (Task 2.1, Proposal Section 5.5.1) in preparation for biodistribution studies planned in Task 2. We selected the gamma emitter  $^{99m}\text{Tc}$ , with a 6.5hr half-life, based on the experience of our collaborators at the University of Texas Health Science Center-San Antonio (UTHSC).  $^{99m}\text{Tc}$  is hydrophilic

and provided as an aqueous solution from the cyclotron source. We originally proposed chelating this radionuclide with a lipophilic chelator, mirroring methods to label liposomes, to facilitate encapsulation using our simple precipitation protocol. This did not work. After examining several commercial chelators, we found both the chelation and the encapsulation efficiency to be very dependent on the 'quality' of the radionuclide.  $^{99m}\text{Tc}$  is subject to oxidation, which affects chelation efficiency, which in turn affects encapsulation efficiency. In most cases, encapsulation efficiency was less than about 20%, which we deemed insufficient. Subsequently, we explored the conjugation of  $^{99m}\text{Tc}$  to reduced proteins, such as bovine serum albumin (BSA), to improve the loading efficiency into nanoparticles. This yielded encapsulation efficiencies of 90% or greater (see Figure 2). Payload stability was monitored over a 24-hour period and was found to be nearly 100%. However, we had concerns about residual reducing agent used to activate the protein interfering with coupling of bone-targeting ligands to functionalized nanoparticles. Therefore, we modified the radiolabeling method to use a commercial reducing gel that can be removed from the protein preparation by simple centrifugation. The newly reduced, clean protein can then be used to complex the radionuclide for encapsulation using the same procedure as before. The encapsulation efficiency is unaffected by this slightly altered approach. Furthermore, this modified method avoids a lengthy column separation process that diminishes the amount of available radioactivity.

We continued work to encapsulate selected proteasome inhibitors and, additionally, to determine drug release profiles from nanoparticle formulations (Task 1.4, Proposal Section 5.4). For example, we encapsulated both PS1 and MG-132, model proteasome inhibitors, using our solvent evaporation protocol with slight modification to improve encapsulation efficiency. Figure 3 shows the resulting payloads for these two drugs, which is about 1% wt. and typical for nanoparticle systems. Release profiles were determined in vitro and it was found that payloads limited to about 1-2% wt. were necessary to achieve a sustained release profile while higher payloads led to an undesirable burst release effect. About 20% of the active drug is released over a period of ten days. Figure 4 shows the typical cumulative release profile of PS1 from two different nanoparticle compositions.

We are currently conducting biological activity assays to determine the activities of release drug. These assays use a combination of a 20S proteasome assay and a cell-based cytotoxicity assay with a human multiple myeloma cell line. This is a simple and convenient enzymatic method for detection of proteasome inhibitors activity. It is based on detection of the fluorophore 7-amino-4-methylcoumarin (AMC) after cleavage from the labeled substrate LLVY-AMC. The cell-based cytotoxicity is performed using the MTT colorimetric assay, which measures the number of living cells after treatment with potential cytotoxic agents. The test consists of treating cultured multiple myeloma cells, such as RPMI8226 or U266, with drug-loaded nanoparticles, empty nanoparticles, or free drug. The nanoparticles are labeled with Rhodamine (see previous discussion) to ascertain nanoparticle fate within the cells.

We are currently conducting in vitro nanoparticle binding studies. Quantification of bone-targeting ligand content on nanoparticle surfaces has been the most difficult aspect of this work to date. The issue is simply that the amount of functional activity on the surface of nanoparticles, either in the form of a functional group (i.e. maleimide) or as attached ligand (e.g. amino bisphosphonate or aspartic acid oligomers), is too small to quantify by methods such as NMR and fluorescent conjugation. Interestingly, this is something that is not addressed in the current literature. Commonly, the existence of targeting ligands is indirectly assessed by the ability of the attached particle to achieve targeting and this is currently how we are assessing the presence of targeting ligands. In our approach, we are conjugating ligands to preformed nanoparticles containing functionalized surfaces and incubating them with hydroxyapatite powders. The nanoparticles are radiolabeled to increase the sensitivity of the assay. One alternative to directly quantify the ligand content is to use radiolabeled ligands, such as with  $^{13}\text{C}$  or  $^{31}\text{P}$ ; however, these materials require custom synthesis, which was not considered in the original statement of work.

Task 2 is concerned with determining the in vivo biodistribution of bone-targeting nanoparticles in myeloma mouse model. The task is broken down into the following subtasks:

1. Prepare radiolabeled bone-targeting nanoparticles – Completed (see above discussion).
2. Conduct in vivo biodistribution assay.

Task 2 has been delayed by difficulties encountered assaying the ligand content of bone-targeting nanoparticles (see previous discussion). The task has been further delayed by a change of venue of our collaborator, Dr. Mundy, who was originally with the University of Texas Health Science Center at San Antonio (UTHSC-SA) and has now moved to new facilities at Vanderbilt University. Dr. Mundy's operations have essentially been down for the past six months and are not expected to be operational until later this Spring. In the meantime, we've been refining our nanoparticle formulations as described above. Furthermore, some of the animals required for the study are diseased and, therefore, cannot be transported the distance from Vanderbilt to UTHSCSA where the biodistribution studies are contracted with the Radiology Department. As such, we have been working with Dr. Mundy to identify a colleague to conduct this portion of the program at the UTHSCSA and still conduct the efficacy studies of Task 3 at Vanderbilt. Presently, we have identified Dr. Mundy's colleague, Dr. Ross Garrett, the program co-PI, to support the biodistribution study animal requirements.



## Key Research Accomplishments

- Developed two procedures for preparing nanoparticles and demonstrated their ability to repeatedly produce nanoparticles with narrow distribution in the target particle size range of 70-200nm and smaller, if necessary.
- Synthesized and fully characterized PLA-b-PEG-Maleimide block copolymers to facilitate the attachment of bone-targeting ligands to polymer nanoparticles via thiol coupling.
- Improved lyostability of polymer nanoparticles, with and without PEG modification.
- Developed methods to radiolabel polymer nanoparticles, the first time, to our knowledge, this has been done.
- Encapsulated two proteasome inhibitors, MG-132 and PS-1, and determined their in vitro release profiles.
- Developed proteasome activity assay to determine activity of encapsulated drug.
- Developing in vitro assay to determine affinity of bone-targeting nanoparticles to hydroxyapatite substrates.

## Reportable Outcomes

- Abstract accepted to Society of Biomaterials Annual Meeting.
- Two abstracts submitted to the Annual Meeting of the Controlled Release Society.
- Invited to present work to the 59<sup>th</sup> Annual Meeting of the Board of Directors of Southwest Research Institute.
- Hired additional professional staff who have been instrumental in completing nanoparticle formulation work and will be supporting upcoming biodistribution studies.
- Subcontract executed for biodistribution study with UTHSC-SA described in Task 2.
- Animal protocols for the biodistribution and efficacy studies described in the original statement of work (Tasks 2 & 3, respectively) have been reviewed and approved by the DoD Animal Care & Use Review Office.

## Conclusions

The completed work positions the project to move into the next task of the project. We can consistently prepare polymer nanoparticles of required size and composition necessary to support other tasks of the project. Technical difficulties encountered during the development of the bone-targeting nanoparticles and the relocation of our collaborator, Dr. Mundy, has delayed the project by about eight months, such that Task 2 remains to be started, but is expected to be started in March.

## References

None.

# Appendix 1

## Figures

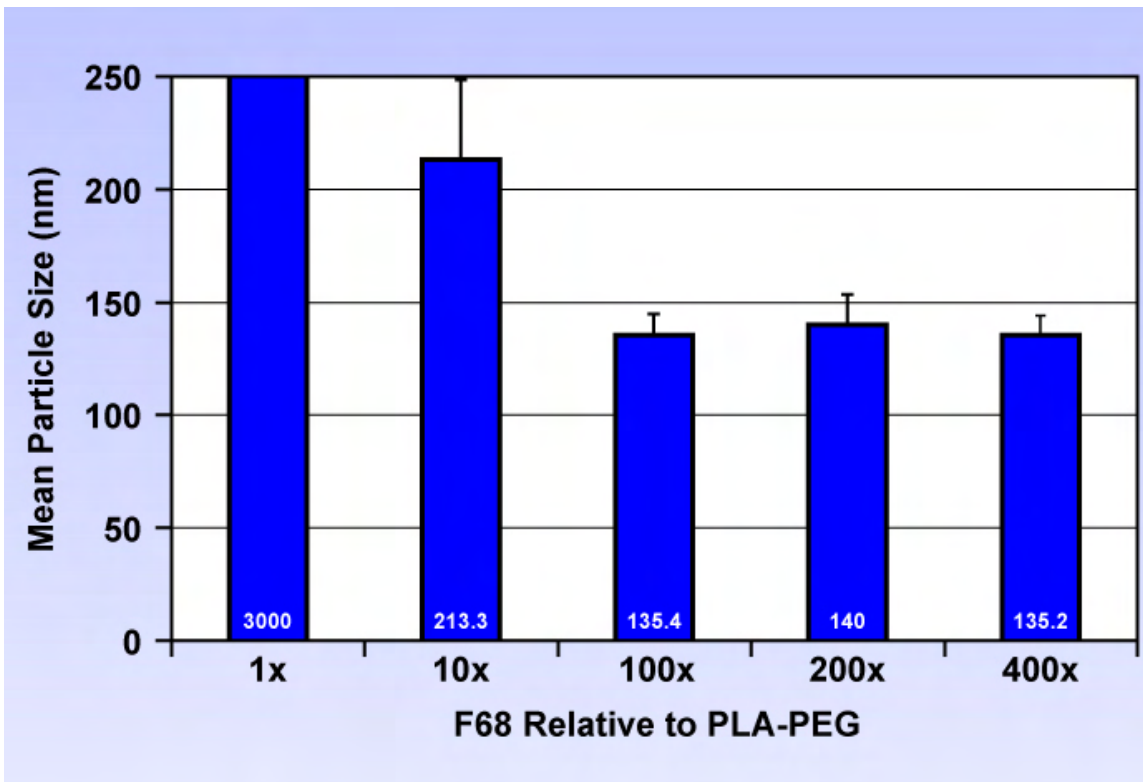


Figure 1. Effect of Pluronic F68 concentration on the lyostability of 90/10 PLGA/PLGA-mPEG nanoparticles.

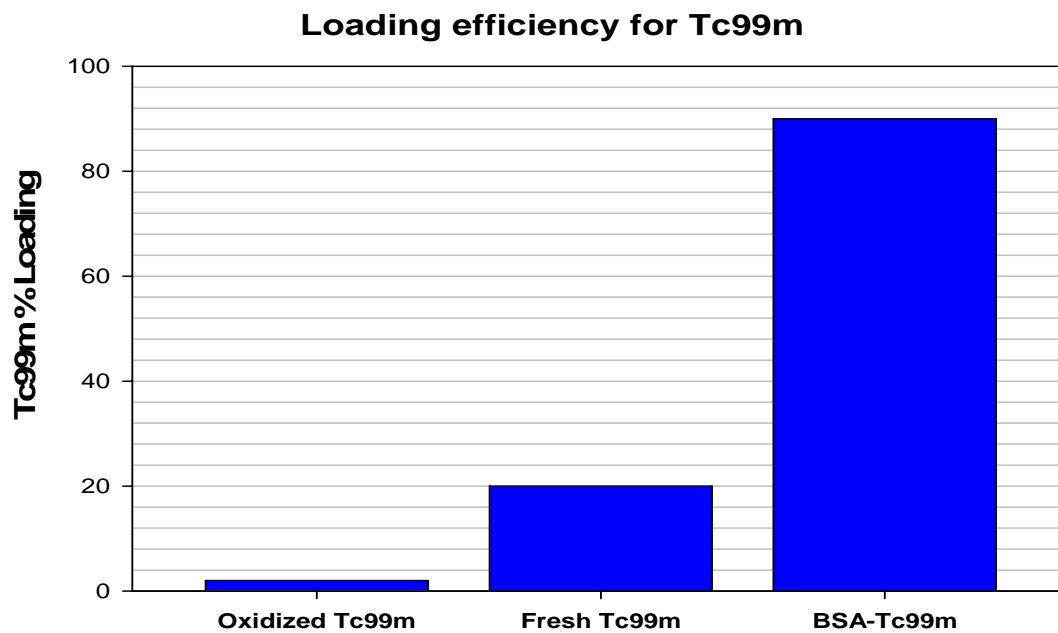
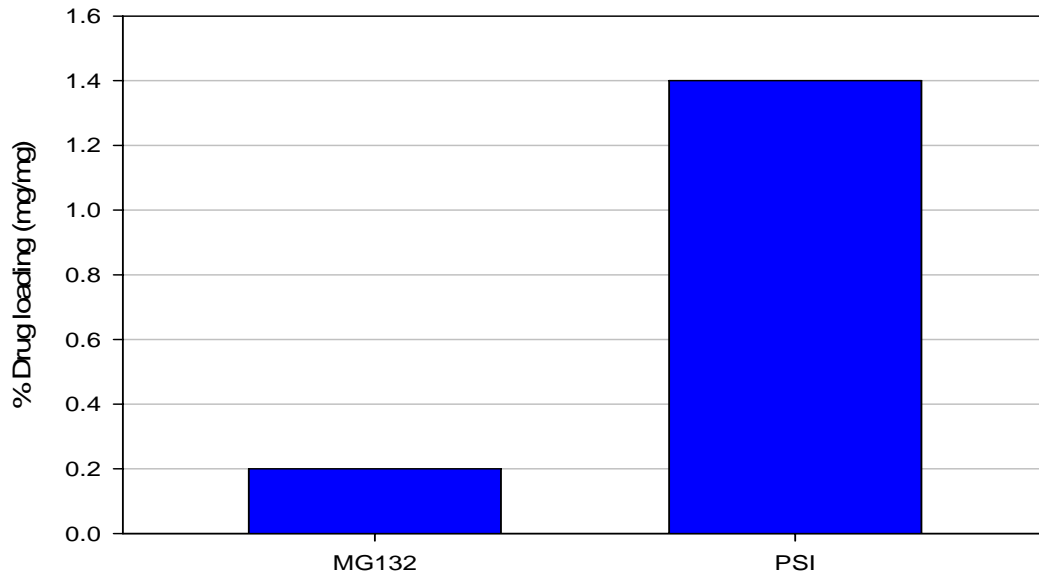


Figure 2. Radiolabeling efficiency of different loading methods. Oxidized  $^{99m}\text{Tc}$  –  $^{99m}\text{Tc}$  chelated with lipophilic ligands and incorporated into nanoparticles by nanoprecipitation. Fresh  $^{99m}\text{Tc}$  – ‘Fresh’ radionuclide chelated with lipophilic ligands and incorporated into nanoparticles by nanoprecipitation. BSA- $^{99m}\text{Tc}$  – Protein-conjugated  $^{99m}\text{Tc}$  incorporated into nanoparticles using a w/o/w emulsion technique.

### Drug loading for two proteasome Inhibitors



**Figure 3.** Encapsulation efficiencies of two proteasome inhibitors.

### Release profile of PSI from nanoparticles

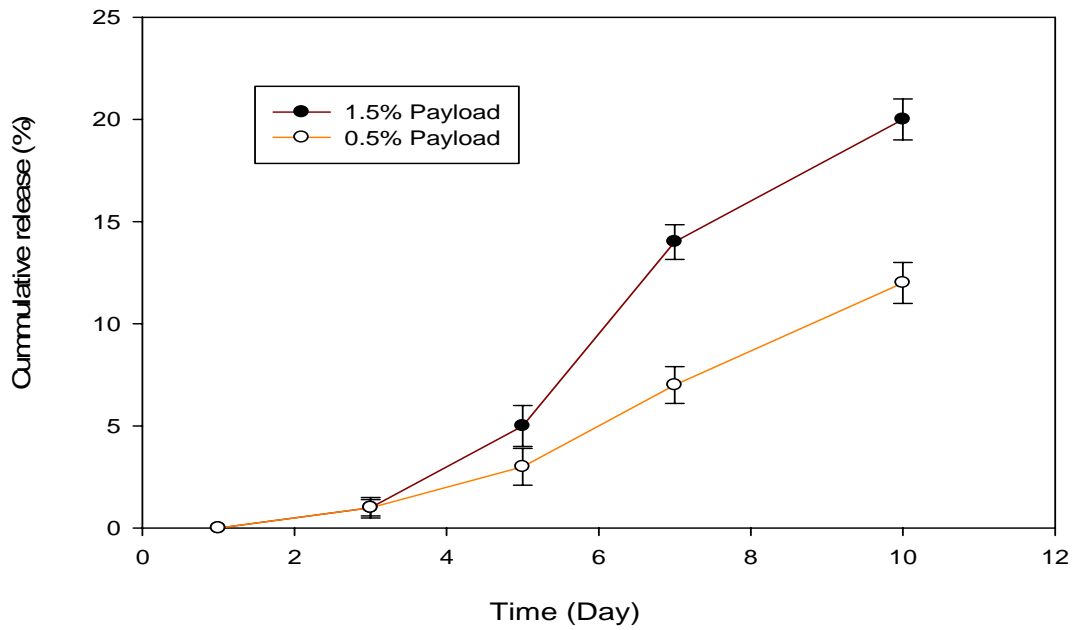


**Figure 4.** Drug release profile for two PS-1 nanoparticle compositions.

# **Appendix 2**

## **NMR Report**

**SwRI**  
**Internal Report**

**Use of NMR to Characterize Reactants and  
Products in DoD Project 01.11300.01.101**

By  
**Dr. Nollie F. Swynnerton**

For  
**Dr. Neal K. Vail**  
**Stefanie M. Crumlett**

**July 25, 2006**

# Use of NMR to Characterize Reactants and Products in DoD Project 01.11300.01.101

## Abstract

Structures of starting materials and products were determined or verified using high-resolution  $^1\text{H}$  NMR. Quantitative  $^{13}\text{C}$  was also used to determine the ratio of PLA to PEG units in the final polymer. Peak assignments were made using predicted chemical shifts, multiplicities, correlation spectroscopy (gCOSY) and selective decoupling. Integration values of the peaks were used in quantification calculations.

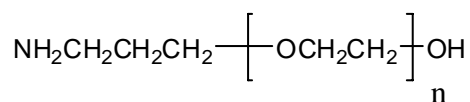
Starting polymer HO-034-PA (**1**) was verified to be poly(ethylene glycol), (PEG), terminated at one end with a 3-aminopropyl group. The average number of ethylene glycol (EG) units per chain was 82. This material was allowed to react with 3-maleimidopropionic acid *N*-hydroxysuccinimide ester to produce amide **2** (MAL-PEG). The isolated crude product was free of starting material by NMR analysis. In an ensuing step, **2** was further polymerized using the lactide 3,6-dimethyl-1,4-dioxane-2,5-dione to append poly(lactic acid), (PLA), to give block polymer **3**. Because the ratio of PLA units to PEG units in **3** was 8.66, this reaction added 710 units of PLA to the 82 units of PEG in the average chain.

## Experimental

(N.B. This section is intentionally detailed to serve as a demonstration of the techniques used in these analyses and as a guide to how one might repeat them or use them in other situations.)

### 1. Determination of the number of EG units in the average polymer chain of 1

The  $^1\text{H}$  NMR spectrum of the starting polymer (at 400 MHz, in  $\text{CDCl}_3$ ) is dominated by the protons of the ethylene bridge units (Figure 1). Vertical and horizontal expansion of the spectrum reveals the multiplets of the terminal aminopropyl moiety (Figures 2, 3). The central methylene of the propyl group is a multiplet centered at  $\delta 1.72$ , the methylene adjacent to the amino nitrogen is a triplet at  $\delta 2.79$ , and the third methylene, which is attached to oxygen, is a triplet on a shoulder of the EG peak and centered at  $\delta 3.55$ . Assignments of the methylene groups were made based on expected chemical shifts and multiplicities. (Note the multiplets at  $\delta 3.46$  and  $\delta 3.81$  flanking the central EG resonance because they will come into play later. They are  $^{13}\text{C}$  satellites and are separated by a one-bond coupling constant ( $^1J_{\text{CH}}$ ) of 140 Hz.) Estimation of the average number of EG units in the starting material was done by comparing the integrals of the terminal aminopropyl methylene groups at  $\delta 1.72$  and  $\delta 2.79$  to the integral of the EG peak. An average of the two integrals was used and the EG integral value was corrected by subtracting the contribution of the methylene attached to oxygen because the separation of the signals was incomplete.



**1, HO-034-PA**

Calculation:

Integral of aminopropyl methylenes =  $(0.58 + 0.62)/4\text{H} = 0.30/\text{H}$

Integral of EG units =  $(98.80 - 0.60)/4\text{H} = 24.55/\text{H}$

Ratio of EG units to terminal units = Average number of EG units per chain

$$= 24.55/0.30$$

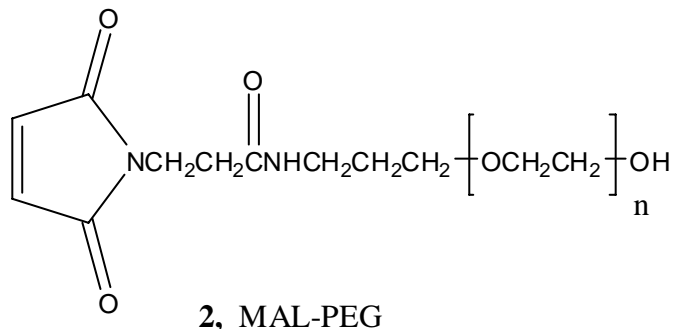
$$= 81.8$$

$$\approx 82$$

Comparison of the integral of a small peak with that of a large peak is subject to a number of variables, so the above value is an estimate. However, several measurements were made with and without spinning (to remove spinning sidebands) and by comparing the integrals of the aminopropyl methylenes with the integral of the EG peak's  $^{13}\text{C}$  satellites (at 0.55% each). Determinations by these techniques varied by only a few units from the above value of 82.

2. Determination of the conversion efficiency of **1** to **2**. Determination of the extent of conversion of starting amine **1** to amide **2** (**2** called MAL-PEG) was approached by first attempting to identify the methylenes of each compound in the  $^1\text{H}$  spectrum of the product. Figure 4 is an expansion of a sample of MAL-PEG which shows that the spectrum is dominated by the EG ethylene units but the expansion reveals the pertinent features of the terminus. There is a multiplet centered at  $\delta 1.76$ , a triplet at  $\delta 2.49$ , a multiplet at  $\delta 3.35$ , and, as determined later, a multiplet centered at  $\delta 3.56$  and a multiplet centered at  $\delta 3.84$ . Although the chemical shifts of the multiplet at  $\delta 1.76$  and the triplet at  $\delta 3.56$  are very close to those of the starting material ( $\delta 1.72$  and  $\delta 3.55$ ), the triplet for the methylene attached to the amine group of the starting material at  $\delta 2.79$  is missing. Instead, there is a multiplet (actually a doublet of triplets) centered at  $\delta 3.35$ . To further characterize the material, it was prudent to identify the separate spin systems. To identify proton-proton spin coupling the 2D COSY experiment<sup>1</sup> has largely replaced homonuclear decoupling<sup>2</sup> in modern practice, but in the study of this system, homonuclear decoupling proved to be extremely useful. This statement can be borne out by examination of the spectra reproduced in Figures 5 – 7. Irradiation of the multiplet at  $\delta 1.76$  and irradiation of the multiplet at  $\delta 3.35$  showed them to be coupled to each other but the triplet at  $\delta 2.49$  was left unperturbed, and therefore not a part of their spin system. Further irradiation of the other peaks allowed the following assignments to be made (refer to structure of **2**):





Central CH <sub>2</sub> of propyl group:	δ1.76
CH <sub>2</sub> adjacent to carbonyl:	δ2.49
CH <sub>2</sub> adjacent to amide nitrogen:	δ3.35
CH <sub>2</sub> adjacent to first EG group:	δ3.56
CH <sub>2</sub> adjacent to imide nitrogen:	δ3.84
Methines of maleimide:	δ6.70

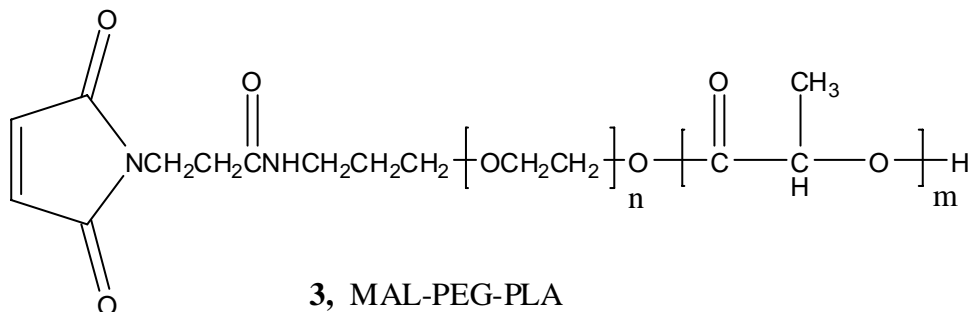
A gCOSY experiment was run on **2**, which confirmed the couplings of the two spin systems. The plot is presented as Figure 8.

The <sup>13</sup>C satellites of **1**, referred to earlier, did not interfere with its analysis by NMR, but the satellites of **2** were found to overlap with the imido methylene group. The homonuclear decoupling experiments and the 2D COSY experiment located the methylene's resonance at δ3.84, but it could not be clearly seen until an experiment was run that decoupled protons from <sup>13</sup>C<sup>3</sup>. As is clear in Figure 9, with the satellites removed the expected triplet of the methyl appears centered at δ3.84 (compare with Figure 10).

That there were no resonances at the chemical shifts of the starting material does not prove that the reaction went to completion, but merely indicates that the material isolated from the reaction mixture was free of starting materials. The conversion *may* have been quantitative or nearly so.

### 3. Determination of the number of poly(lactic acid) (PLA) in product **3**

Reaction of **2** with 3,6-dimethyl-1, 4-dioxane-2, 5-dione appended a polyester chain to the PEG terminus, but it remained to determine the average number of PLA units in the chain. Integrals of the resonances of the methyl groups and the methine groups of the isolated product **3** were compared with the integral of the EG ethylene groups to provide the answer. Figure 11 is a <sup>1</sup>H NMR spectrum of **3**, (called MAL-PEG-PLA). Three patterns dominate the spectrum; the methyl groups of the PLA portion of the molecule are centered at δ1.58, the methines of PLA are grouped at δ5.2 and the ethylenes of PEG are at δ3.64. The ratio of the methyls to the methines is high, 3.26:1, but there is an underlying "hump" in the spectrum that interferes positively with the integration of methyls. Comparison of the integral of the methines with the integral of the PEG ethylenes and correcting for the number of protons in each moiety gave a ratio of PLA units to PEG units of 8.66.



Quantitative  $^{13}\text{C}$  was also investigated as a tool to estimate the PLA:PEG ratio. A sample was made up to contain 10 mg/mL of chromium (III) acetylacetonate  $[\text{Cr}(\text{acac})_3]$  as a relaxation agent and inverse gated decoupling was used to suppress the nuclear Overhauser enhancement (nOe). Using this technique a ratio of 6.78 was obtained. The close proximity of the PEG resonances to the methine of PLA made integration difficult, so the result obtained from the  $^1\text{H}$  integration is likely to be the better estimate.

### Future Work

Amide **3** is to be converted into nanoparticles with the PEG polymer chains remaining external to the central sphere. Characterization of this material may possibly be done using NMR and our nanoprobe, and the attached section of a textbook may be useful as a starting place. Solid-state NMR has also been used<sup>5</sup> to characterize similar systems, and we have such capability.

### EndNotes

1. The 2D COSY experiment can easily be done using the “walkup” feature of the spectrometer. It can also be done with a little more control of the variables, especially the plotting, from the “experimental” mode. Directions on how to do this are in the green manual under “2D COSY”.
2. Directions on how to do homonuclear decoupling (spin-spin decoupling) are in the green book under “Homonuclear decoupling”.
3. Decoupling of carbon 13 from protons is described in the green book under “C13 decoupling”.
4. Quantitative  $^{13}\text{C}$  can be done if the slow relaxation of the spins is treated and if the nuclear Overhauser effect (nOe) is suppressed. The former is negated by using a relaxation agent, in this case chromium acetyl acetonate,  $\text{Cr}(\text{acac})_3$ , and the latter is removed using inverse gated decoupling, in which the decoupler is gated on only during the acquisition time, with a succeeding delay in the pulse train.
5. C.R. Heald, et al., *Langmuir*, 18, 3669-3675.

# Figures

SMC 051006  
HO-PEG-NH2

File: SMC\_HOPEGNH2\_H  
Pulse Sequence: s2pu1  
Solvent: cdcl3  
Temp. 24.0 C / 297.1 K  
Operator: SwynerT  
File: SMC\_HOPEGNH2\_H  
INOVA-400 "swrinmr2"

Relax. delay 5.000 sec  
Pulse 22.5 degrees  
Acq. time 2.048 sec  
Width 6400.0 Hz  
& repetitions  
OBSERVE H1, 399.8060023 MHz  
DATA PROCESSING  
Line broadening 0.2 Hz  
FT size 65536  
Total time 0 min, 56 sec

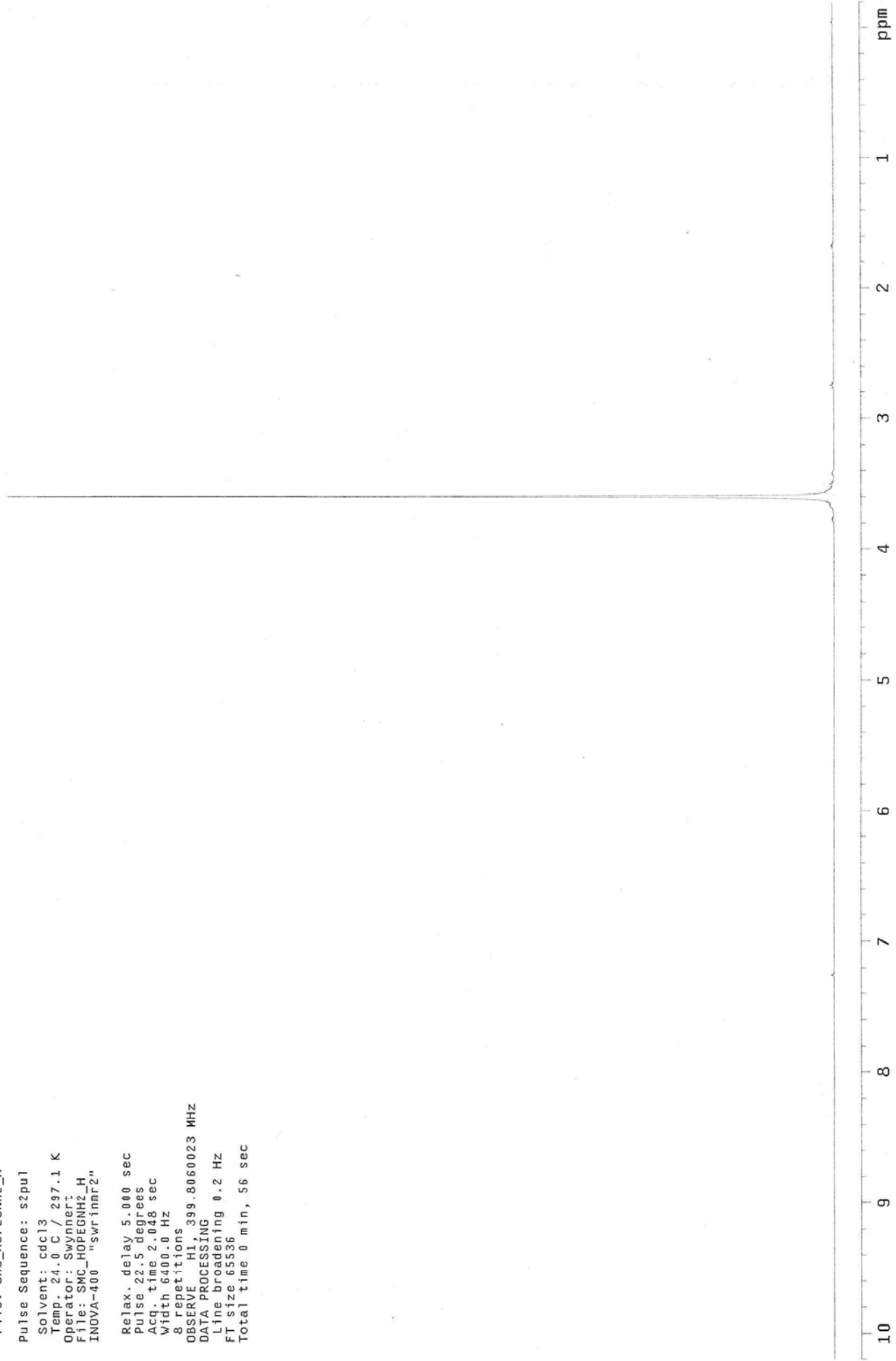


Figure 1. <sup>1</sup>H NMR spectrum of HO-034-PA showing predominance of -OCH<sub>2</sub>CH<sub>2</sub>O- groupings

SMC\_051006  
HO-PEG-NH2

File: SMC\_HOPEGNH2\_H

Pulse Sequence: s2pul

Solvent: cdcl3

Temp. 24.0 C / 297.1 K

Operator: Swymer

File: SMC\_HOPEGNH2\_H

INOVA-400 "swrinmr2"

Relax. delay 5.000 sec

Pulse 22.5 degrees

Acq. time 2.048 sec

Width 6400.0 Hz

8 repetitions

OBSERVE H1, 399.8060023 MHz

DATA PROCESSING

Line broadening 0.2 Hz

FT size 65536

Total time 0 min, 56 sec

VS X100

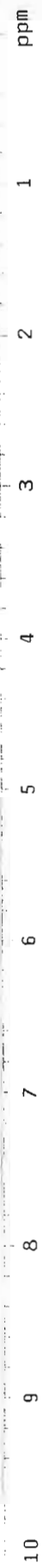


Figure 2. <sup>1</sup>H NMR spectrum of HO-034-PA with vertical expansion showing end-group resonances

SMC\_051006  
HO-PEG-NH2

exp21 s2pu1

```
SAMPLE SPECIAL 24.0
date May 10 2006 temp
solvent cdcl3 gain 26
file not used
ACQUISITION exp hst 0.0008
sw 3254.7 pw90 14.500
at 2.048 a1ra 6.600
np not used fl
fb 13334 n
bs 32 in
di 5.000 dp n
nt 8 hs nm
ct TRANSMITTER 8 lb PROCESSING 0.201
tn HI fn 65536
sfrq 399.807
tof -566.2 sp DISPLAY 285.28
tpwr 52 wd 1545.4
pw DECOUPLER 3.625 rfl 175.4
dn 99.8 rf0
dof 0 rp -7.3
dm nnn ip
dmm c wc 250
dpwr 40 SC 0
dmf 17094 VS 5070
at ph 41
```

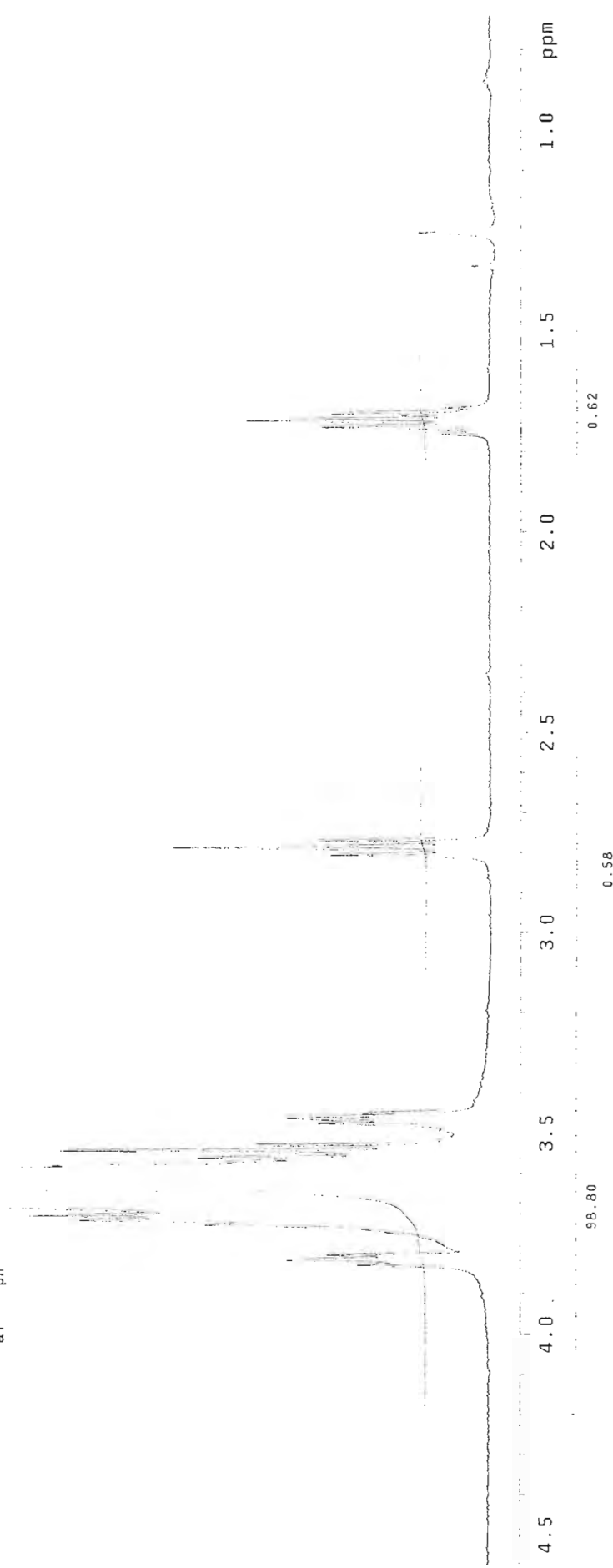


Figure 3. Expanded <sup>1</sup>H NMR spectrum of HO-PEG-PA, showing methylene resonances of aminopropyl end group

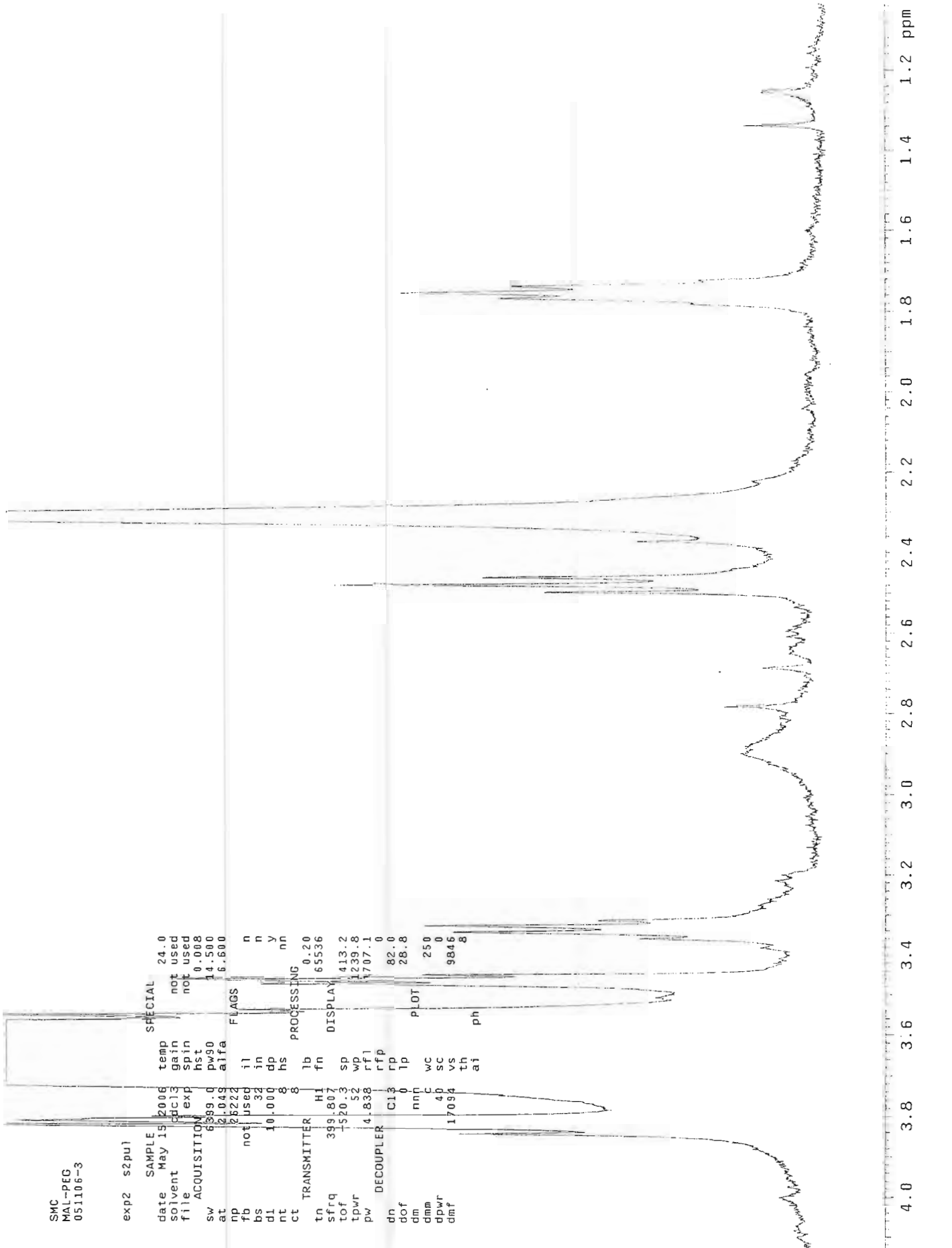
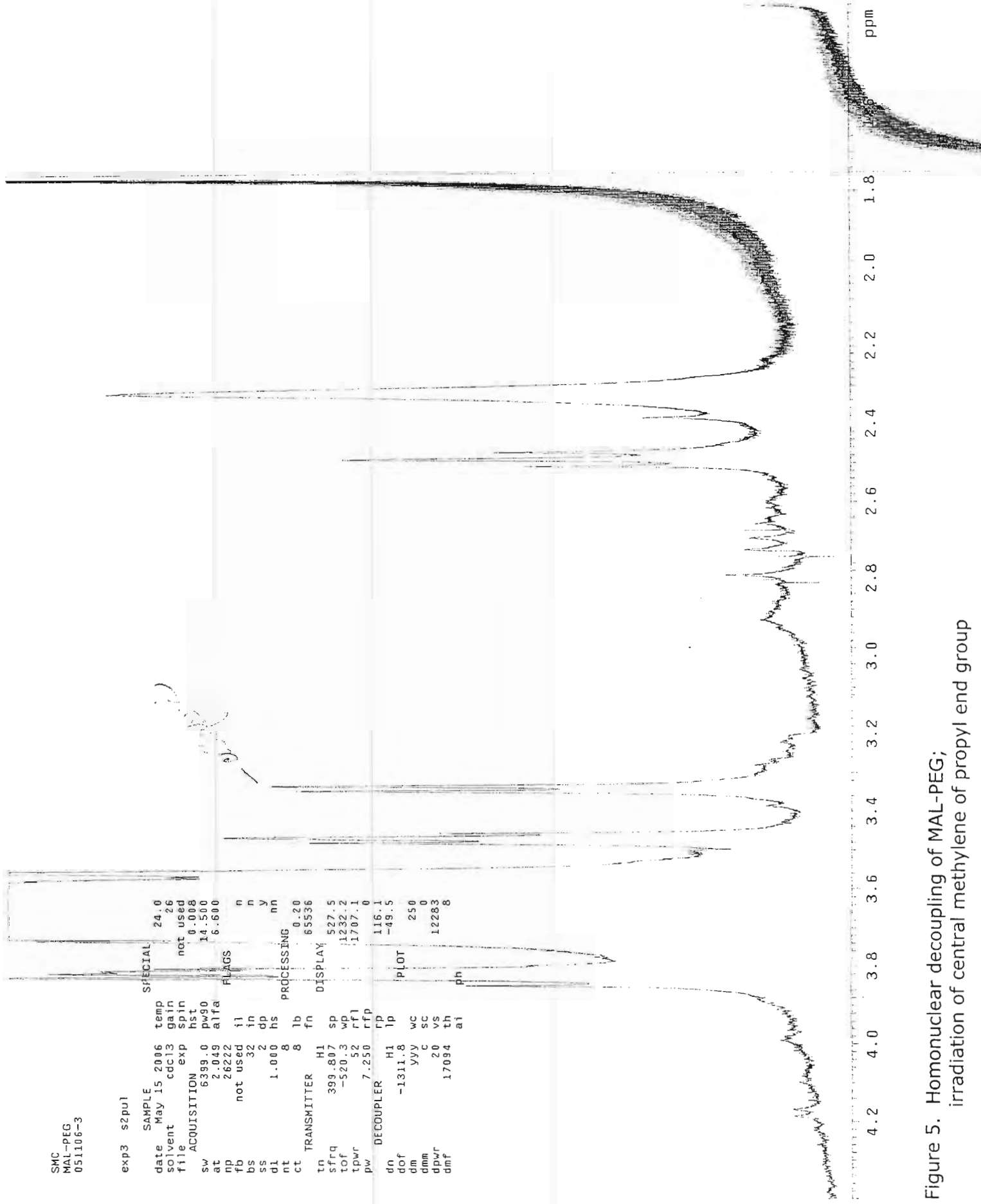


Figure 4. Expanded <sup>1</sup>H NMR spectrum of MAL-PEG, showing end-group resonances



SMC  
MAL-PEG  
051106-3

exp3 s2pul

date	May 15 2006	temp	24.0
solvent	cocl3	gain	26
file	exp	not used	
ACQUISITION	exp	hst	0.008
sw	6389.0	pw90	14.500
at	2.049	alfa	6.600
np	not used	fl	n
fb	26222	in	n
bs	32	in	y
ss	2	dp	nn
dl	1.000	hs	
nt	8	PROCESsing	nn
ct	8	lb	0.20
TRANSMITTER	H1	fn	65536
In		DISPLAY	
sfrq	399.807	sp	527.5
tof	-520.3	wp	1232.2
tpwr	52	rfl	1707.1
pw	7.250	rfp	0
DECOUPLER	rp		116.1
dn	H1	lp	-49.5
dof	-1311.8	PLOT	
dm	yyv	wc	250
dmm	yy	sc	0
dppr	20	vs	12283
dmf	17094	th	8
		ai	

Figure 5. Homonuclear decoupling of MAL-PEG; irradiation of central methylene of propyl end group



SMC  
MAL-PEG  
0511106-3

exp4 s2pul

```

SAMPLE
date MAY 15 2008
solvent CDCl3
file exp
ACQUISITION
sw 6399.0
at 2.08
np 2624
fb not used
bs 32
dl 1.000
nt 8
ct TRANSMITTER HI
tn 391.897
sfrq -520.3
tof 52
tpwr 7.250
pw DECOUPLER HI
dn -1021.2
ref 28.8
em 250
Qzella 0
d15wr 9845
dhrf 17094
ai ph

```

```

SPECIAL
temp 24.0
gain not used
spin not used
hst 0.008
pw90 14.500
alfa 6.600
n
n
y
nn
PROGRESSING
lb 0.20
fn 6556
DISPLAY
sp 413.2
wp 1239.8
rf1 1707.1
rfp 0
fp 78.7
lp 28.8
PLOT
wc 250
sc 0
vs 9845
th 8
ai ph

```

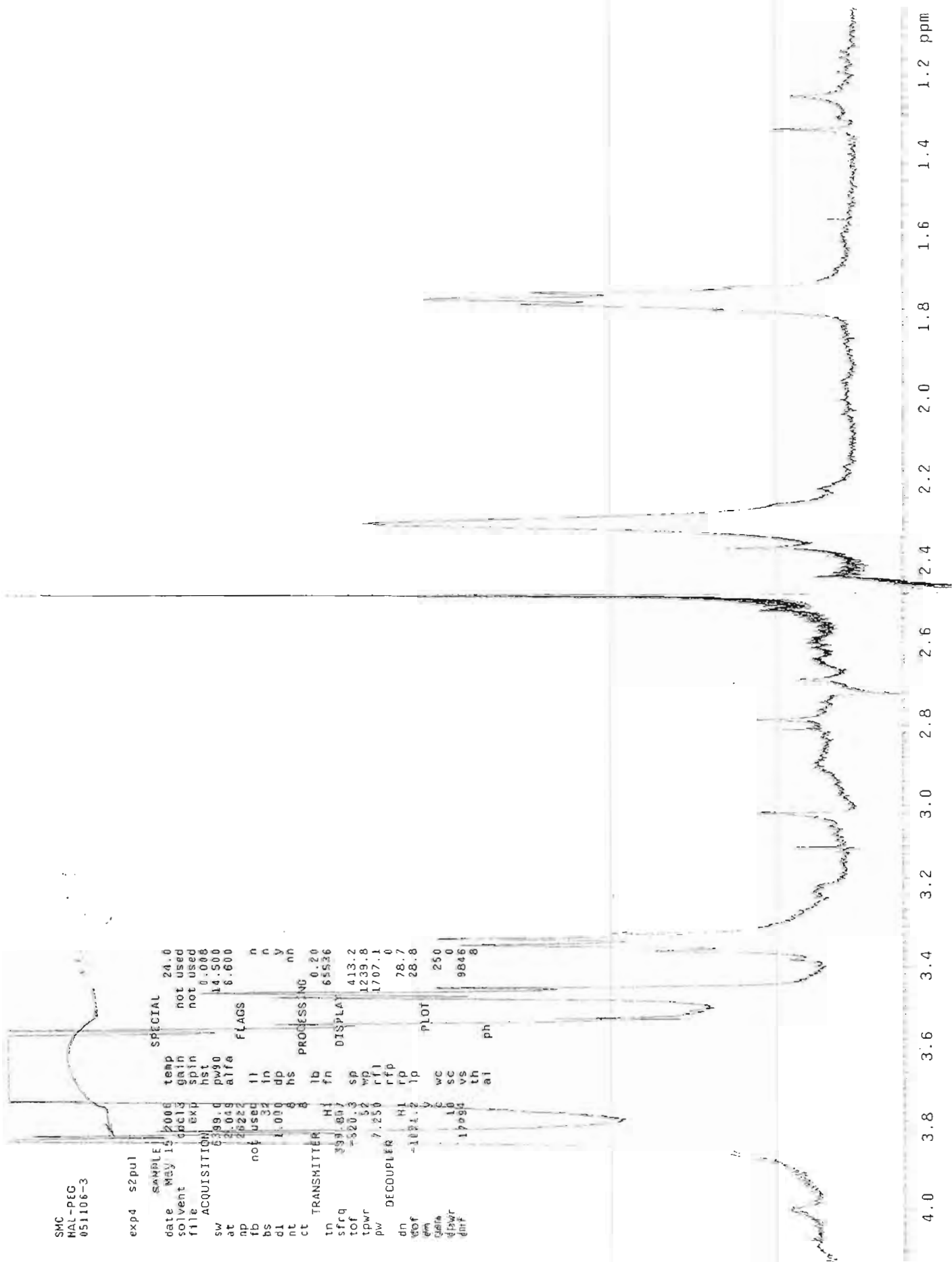


Figure 6. Homonuclear decoupling of MAL-PEG; irradiation of multiplet at 2.5 ppm; collapse of multiplet at 3.84 ppm

SMC  
MAL-PEG  
051106-3

exp9 s2 pu1

SAMPLE SPECIAL 24.0  
date Jun 9 2006 temp 30  
solvent cdc13 gain 30  
file cdc13 not used  
ACQUISITION exp hst 0.008  
sw 6399.0 pwsb 17.500  
at 2.049 alfa 6.600  
np not used 11 n  
fb 26222 18 in n  
cl 54 0 dpl y  
nt 54 hs  
cl 54 PROCESSING nn  
TRANSMITTER lb 0.20  
fn 55336  
sfrq 399.807 DISPLAY 594.2  
tof -520.3 sp 1064.9  
tpwr 52 wd 1707.1  
pw 7.20 rfb 0.08.4  
DECOUPLER rl rp 5.1  
dn -479.3 lp  
dm y/y wc 250  
dmc C SC 0  
dpwr 5 vs 10238  
dmf 17054 th 2  
al ph

← collapsed  
triplet

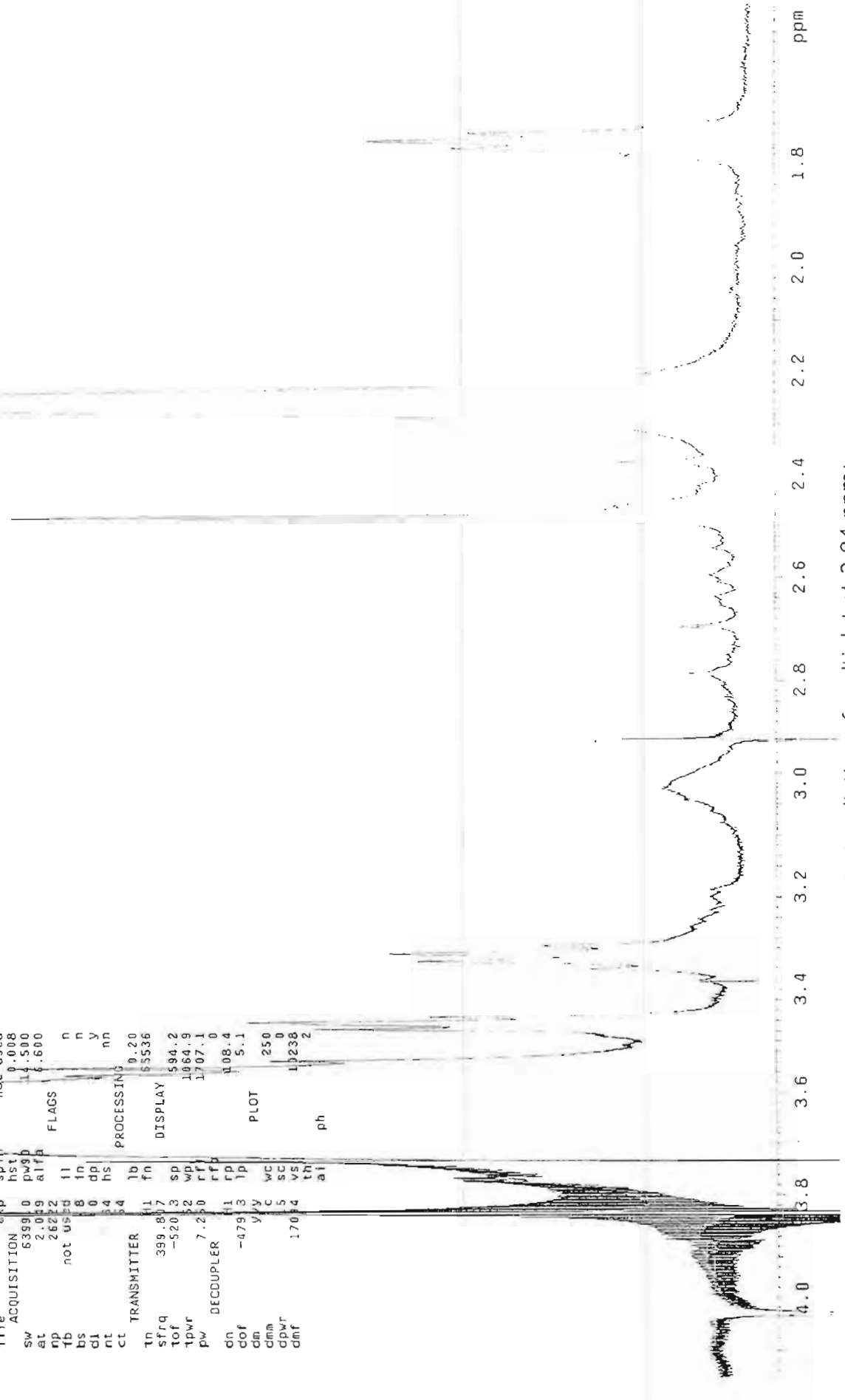


Figure 7. Homonuclear decoupling of MAL-PEG; irradiation of multiplet at 3.84 ppm;  
collapse of multiplet at 2.5 ppm

SMC  
MAL-PEG  
051106-3

Automation directory:

Pulse Sequence: gCOSY  
Solvent: cdcl3  
Temp. 24.0 C / 297.1 K  
Operator: Swnnert  
INOVA-400 "swr1nmr2"

Relax. delay 1.301 sec  
Acq. time 0.144 sec  
Width 3543.6 Hz  
2D Width 3543.6 Hz  
Single scan  
256 increments  
OBSERVE H1, 399.8060023 MHz  
DATA PROCESSING  
Sq. sine bell 0.072 sec  
F1 DATA PROCESSING  
Sq. sine bell 0.072 sec  
FT size 4096 x 4096  
Total time 6 min, 45 sec

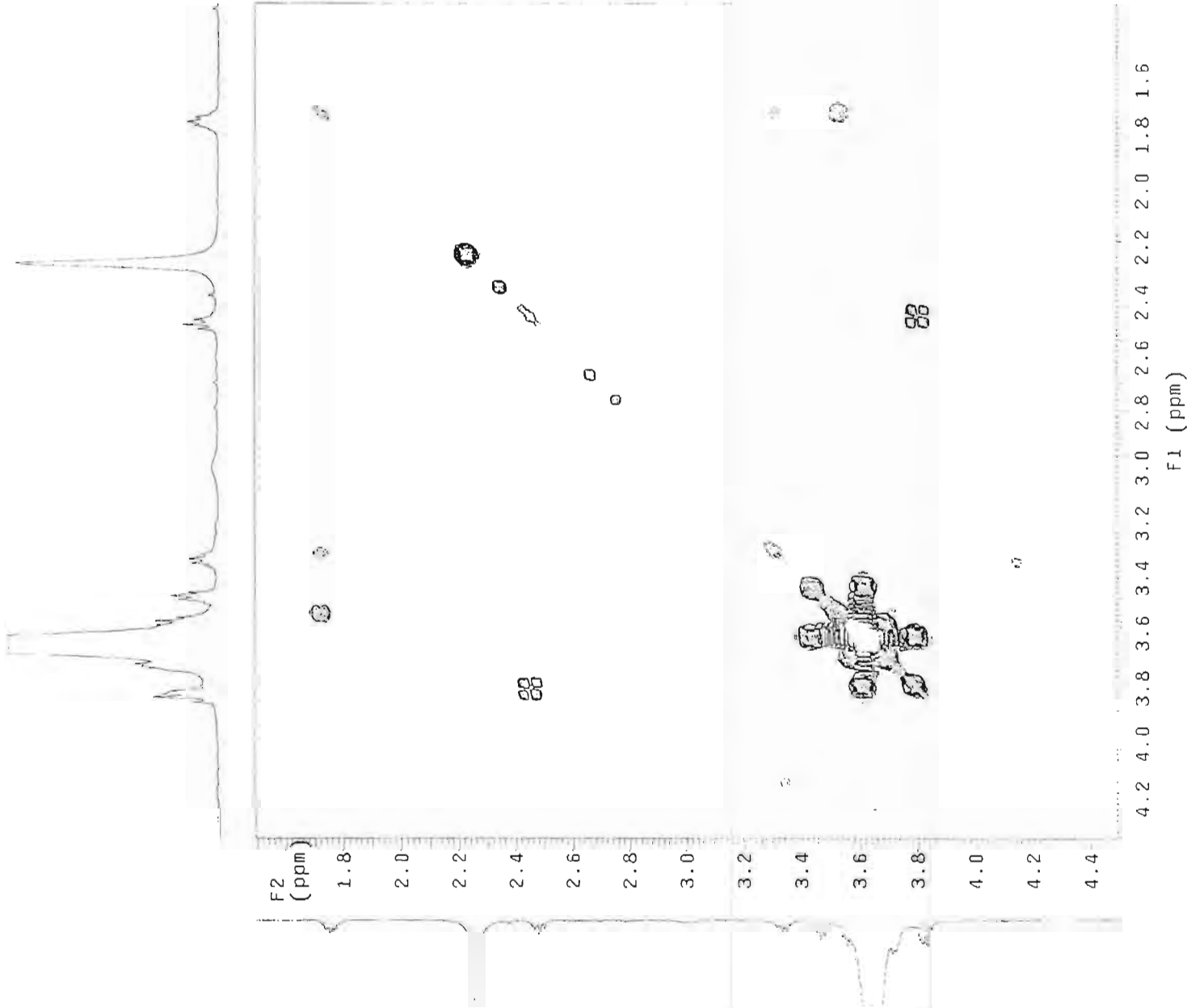


Figure 8. gCOSY spectrum of MAL-PEG

*Decoupled from  $^{13}\text{C}$  to remove satellites*

SMC  
MAL-PEG  
051106-3

```

exp3 szpul
SAMPLE
date Jun 10 2006 temp 24.0
solvent cdc13 gain not used
file exp sbin 20
ACQUISITION
sw 6399.0 fwh0 14.500
at 2.046 a1fa 6.600
np not used l l n
fb 8 th n
bs 2 dp y
ss 0 hs nn
d1 64 lb 0.20
nt 60 fn 65536
ct TRANSMITTER HI DISPLAY
tn 395.807 sp 622.0
sfrq -520.3 wp 1003.4
tof 52 rf1 1708.3
pwr 7.250 rfp 0
pw DECOUPLER C13 lp 138.9
dn 3.9
dof 0 wc 250
dm vvy g sc 0
dmm 40 vs 10027
dpr 1709.4 th ai 3
dmf ai ph
  
```

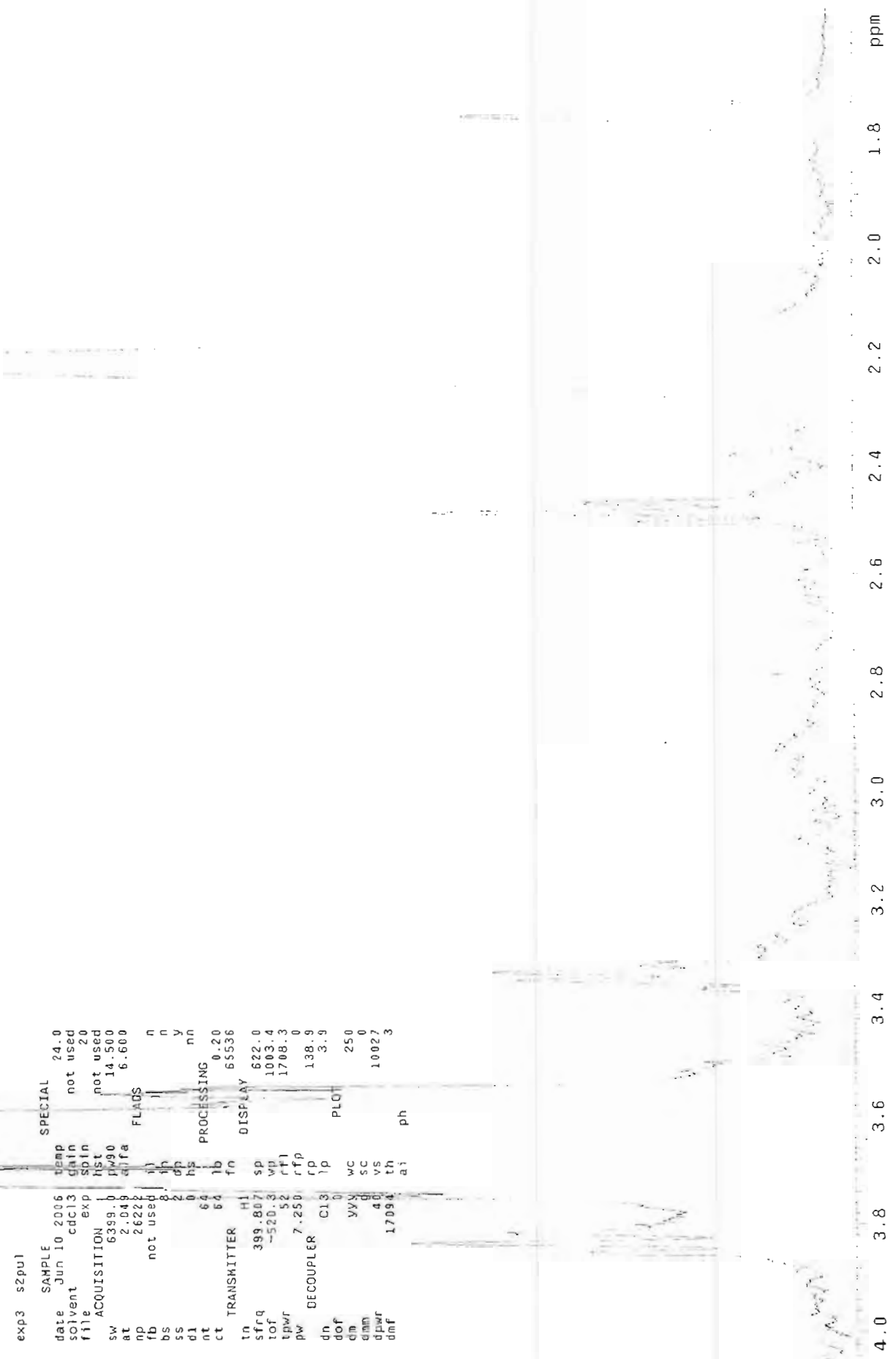


Figure 9.  $^1\text{H}$  NMR spectrum of MAL-PEG with  $^{13}\text{C}$  decoupling; removal of  $^{13}\text{C}$  satellites allows unobstructed view of end-group methylene at 3.84 ppm (compare with Figure 10)

SMC  
MAL-PEG  
051106-3

exp2 s2pu1

date	Jun 10 2006	temp	24.0
solvent	cdcl3	gain	not used
file		spin	20
ACQUISITION		hst	not used
sw	6399.0	pw30	14.500
at	2.049	al7a	6.600
np	26222	FLAGS	
fb	not used	il	n
bs	32	ih	n
d1	0	dp	y
nt	32	ws	nn
ct	32	PROCESSING	
IN	TRANSMITTER	fb	0.50
to	H1	fn	65536
sfrq	399.807	DISPLAY	
tof	-520.3	sp	622.0
tpwr	52	wp	1003.4
pw	7.250	rf1	1708.3
DECOUPLER	C13	rf2	0
dn	PP	rfp	120.4
def	0	rp	3.9
d1a	nan	PLOT	
d1m	C	WC	250
d1m2	40	SC	0
epwr	17054	VS	1828
d1m1		th	3
		ph	

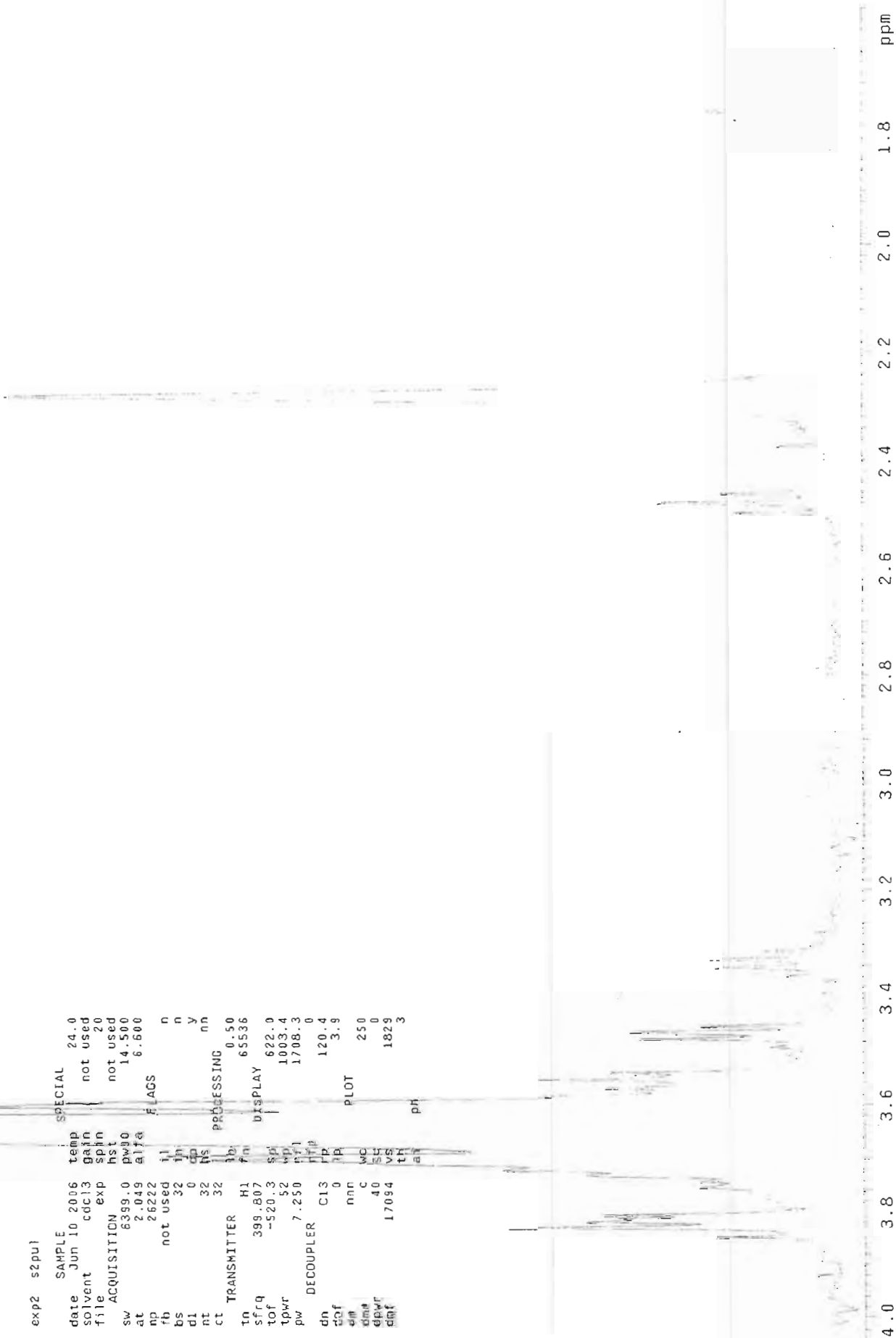


Figure 10. Expanded <sup>1</sup>H NMR spectrum of MAL-PEG; all five methylenes of end group clearly visible

SMC  
MAL-PEG-PLA

exp8 szpul

```

SAMPLE
date Jun 1 2006 temp 24.0
solvent cdcl3 gain not used
file exp 20
ACQUISITION hst 0.008
sw 6399.0 pw90 13.000
at 2.048 alfa 6.600
bs not used il FLAGS
ss 26222 32 in n
d1 1.000 hs y
nt 16 fn PROCESSING nn
ct TRANSMITTER 16 fn DISPLAY 65536
tn
sfrq 399.807 wp 3322.7
tof -801.5 rfi 1995.8
tpwr 53 rfp 0
pw 4.338 rp 104.6
DECOUPLER C13 lp 4.6
dn
dof 0 wc 250
dm nnn sc 0
dmm c vs 101
dppr 40 th 12
dmf 17094 ai ph

```

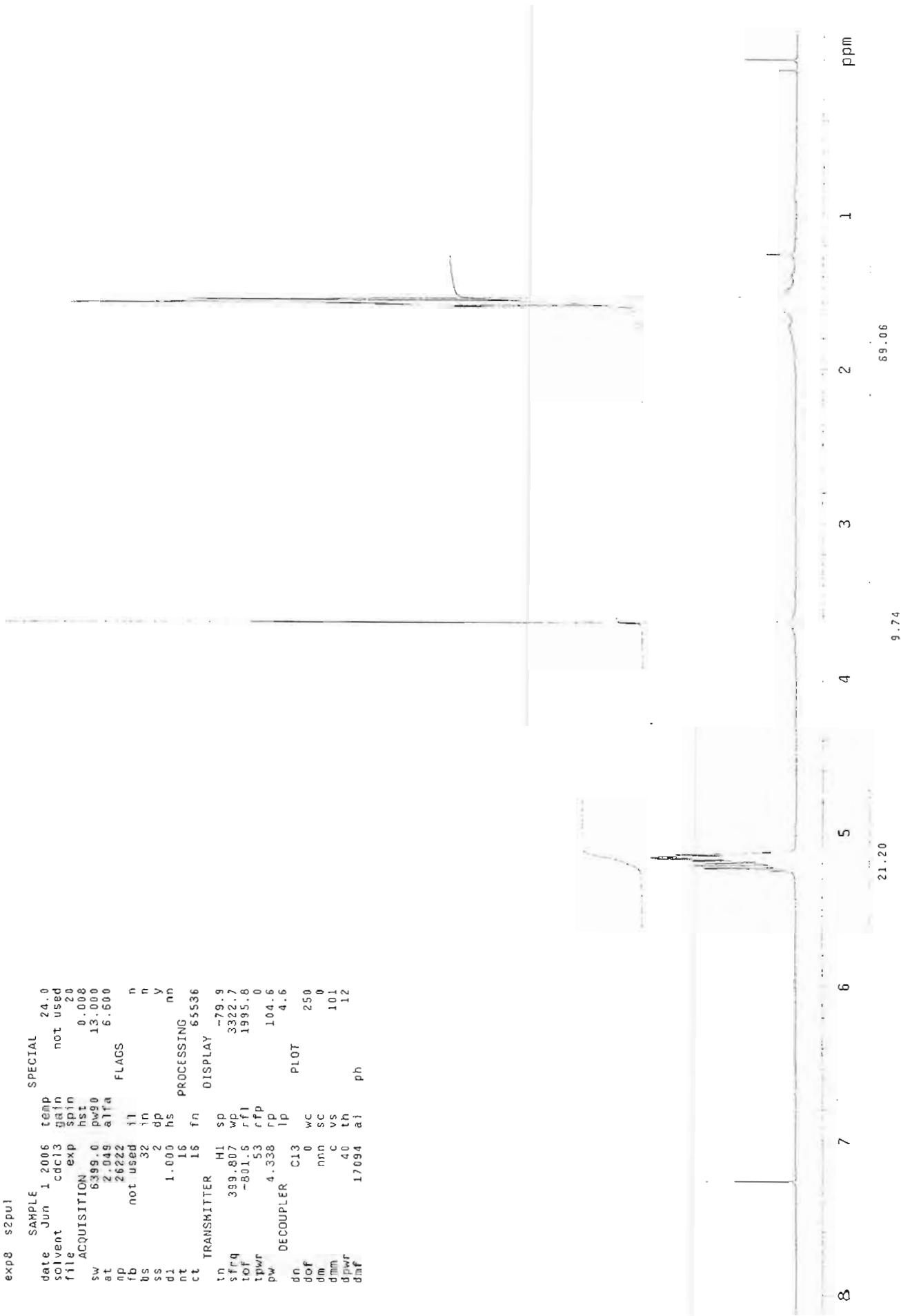


Figure 11. <sup>1</sup>H NMR spectrum of MAL-PEG-PLA; integration of resonances allows calculation of average number of repeating units in each copolymer segment

# **Appendix 3**

## **Abstracts**

## Development and Characterization of Bone-Targeting Nanoparticles

Stefanie Crumlett, Gianni Rossini, M.S., Jack Trevino, Neal Vail, Ph.D.

Biomaterials Research, Southwest Research Institute, San Antonio, TX 78238

stefanie.crumlett@swri.org

### Abstract Summary:

We have developed and characterized biodegradable, polymeric nanoparticles for the purposes of providing targeted delivery of therapeutic agents to bone. We further demonstrate the encapsulation of a gamma emitting radiolabel for the use in future in vivo biodistribution.

### Introduction:

In previous work, we prepared ligand-containing liposomes and showed these nanocapsules preferentially adhered to hydroxyapatite substrates in vitro[1]. However, encapsulating hydrophobic actives in liposomes is problematic. Therefore, we turned to polymer nanoparticles as an alternative. Nanoparticles with a hydrophobic core and hydrophilic corona have shown excellent anti-immunogenic properties. The hydrophilic property of polyethylene glycol (PEG) and the hydrophobic property of poly lactic acid (PLA), poly glycolic acid (PGA), and their copolymer (PLGA) optimize the stealth-like capabilities of the nanoparticles as well the sustained release of drug therapy. The ability to target to bone will reduce the toxic systemic exposure of some therapies as well as increase the efficacy of the therapy in bone. A bone-targeting ligand can be chemically attached to the surface of the nanoparticles. The calcium matrix of bone makes for an exceptional delivery target. We have identified bone-binding ligands which have previously shown tendency toward bone. We chose two molecules, methylene bisphosphonate (MBP) [2] and an Aspartic Acid oligopeptide ( $Asp_{(n)}$ ) [3], as our bone-targeting ligands. We present the development and characterization of a biodegradable block-copolymer and bone-targeting nanoparticles.

### Methods:

#### *Synthesis of Ligand Coupled Block-Copolymer*

Poly(lactide-co-glycolide) (PLGA, 75/25, Brookwood) was used to prepare nanoparticles. Functional polyethylene glycols (PEG) were obtained from NOF Corp.  $Asp_4$  was obtained from Sigma. PLGA-b-PEG was prepared by conjugating PLGA to an amine-terminated mPEG via DCC/NHS coupling. Maleimide-terminated PEG-b-PLA copolymer was prepared by ring-opening polymerization of lactide on to a hydroxyl-terminated bifunctional PEG. Maleimide was added to the PEG terminus by reaction with 3-maleimidopropionic acid NHS ester. Amino-MBP was synthesized by modified reported method [4]. Either aMBP or  $Asp_n$  was linked via sulfhydryl-amino conversion to the functionalized copolymer. Ligand conjugation was monitored by sulfhydryl UV-detection method. All structures were confirmed by  $^1H$ -NMR.

#### *Preparation and Lyophilization of Nanoparticles*

Nanoparticles were prepared by either emulsification/solvent-loss or nanoprecipitation. Solvent was removed by evaporation. Particles were purified by ultracentrifugation or cross-flow filtration and lyophilized. Several lyo-protectants were studied to help prevent nanoparticle agglomeration, including sugars [5] and pluronics. Particle size was determined by photon correlation spectroscopy and zeta-potential measured at pH 7.4.

#### *Encapsulation of $^{99m}Tc$*

Encapsulation of  $^{99m}Tc$  was studied using either a lipophilic chelator (e.g. Ceretec<sup>TM</sup>) or a protein-conjugate as a means stabilize the radionuclide in the nanoparticles. Chelation was conducted and confirmed according to kit instructions. Protein conjugation was done using Bovine Serum Albumin (BSA). The protein sulfhydryl groups were reduced with  $NaBH_4$  and subsequently conjugated to  $^{99m}Tc$  pertechnetate ions using a stannous chloride catalyst.

#### *Binding Assay*

Preferential binding of ligand-containing nanoparticles to hydroxyapatite substrates was determined using  $^{99m}Tc$  radiolabeled nanoparticles. Nanoparticles with and without ligands were exposed to high surface area hydroxyapatite powders (DNA grade Bio-Gel Hydroxyapatite, Bio-Rad) at physiological pH and temperature at varying concentrations for approximately one hour. The suspensions were centrifuged, the supernatant was decanted and the radioactivity of the supernatant and pellet were measured. The nanoparticle adsorption was calculated by mass balance.

### Results/Discussion:

Nanoparticles were prepared from PLGA/PLA-PEG blends. Nanoparticles prepared by emulsification ranged in size from 150nm to about 200nm, depending on the PEG content, with particle size decreasing with increasing PEG content. Similarly, zeta-potential decreased with increasing PEG content, suggesting shielding of the PLGA surface by the surface PEG groups, although nanoparticle dispersion stability was not affected. Nanoparticles prepared by nanoprecipitation ranged in size from about 75nm to about 150nm, depending on solvent choice, polymer concentration, and PEG content.

$^1H$  NMR of the custom synthesized maleimide-PEG-b-PLA polymer indicated the PLA segment had a length of about 710 units, or a  $M_w$  of about 50k. Attachment of the maleimide group had a conversion of 100% and ligand attachment to the maleimide was similarly determined to occur with high conversion.



Polymer nanoparticles are known to agglomerate during lyophilization. We found certain sugars to provide lyo-protection, but only at significant concentrations (e.g. greater than 20% wt.). We found pluronic F68 to be a more effective lyo-protectant at concentrations equivalent to the polymer nanoparticle content (e.g. ~1% wt. or less)(figure 1).

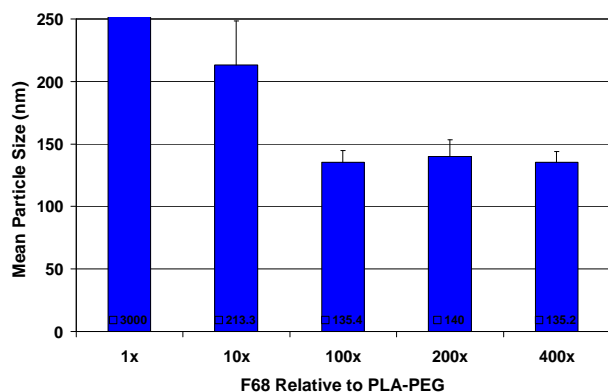


**Figure 1.** Effect of Pluronic F68 on redispersion of lyophilized nanoparticles.

The chelation efficiency of lipophilic chelators was over 90%; however, this was very sensitive both to the age of the  $^{99m}\text{Tc}$  and to the chelation conditions.  $^{99m}\text{Tc}$  is subject to oxidation, which can deleteriously affect chelation. Therefore, it was important to use ‘fresh’  $^{99m}\text{Tc}$  within about two hours after milking from the cyclotron. However, even with fresh  $^{99m}\text{Tc}$ , the encapsulation efficiency was still low, typically 20% or less. Protein conjugation proved much more efficient, providing nanoparticles with high loading and more suitable for future in vivo biodistribution studies (figure2).

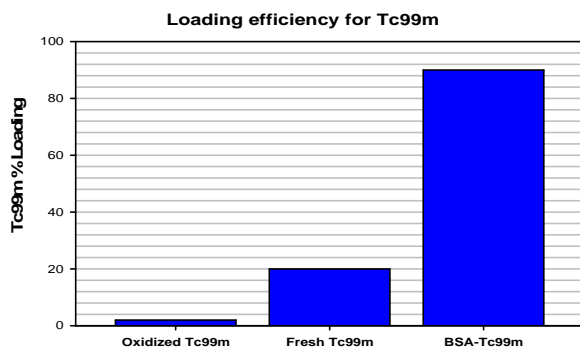


**Figure 2.** Radiolabeling efficiency of different loading methods. Oxidized  $^{99m}\text{Tc}$  –  $^{99m}\text{Tc}$  chelated with lipophilic ligands and incorporated into nanoparticles by nanoprecipitation. Fresh  $^{99m}\text{Tc}$  – ‘Fresh’ radionuclide chelated with lipophilic ligands and incorporated into nanoparticles by nanoprecipitation. BSA- $^{99m}\text{Tc}$  – Protein-conjugated  $^{99m}\text{Tc}$  incorporated into nanoparticles using a w/o/w emulsion technique.

The preferential adherence of these ligand-containing, radiolabeled nanoparticles was evaluated with crystalline hydroxyapatite powder. Attachment of ligand-containing nanoparticles was found to occur in a Langmuir-like behavior. Nanoparticles without targeting ligands had no significant affinity for the HAp substrates.

### Conclusion:

In this study, we developed and characterized ligand-terminated, biodegradable polymers, and formulated bone-targeting nanoparticles using these materials. We prepared lyo-stable nanoparticles. We demonstrated the high-efficiency encapsulation of  $^{99m}\text{Tc}$  as a protein conjugate. We showed the preferential adherence of  $^{99m}\text{Tc}$ -labeled nanoparticles containing bone-targeting ligands to hydroxyapatite substrates *in vitro*. Bone-targeting technology has potential for many skeletal diseases such as osteoporosis, tumor therapy, fracture repair, and bone pain.

### References:

1. Vail, et al, CRS 2003
2. Davis, et al., Semin Nucl Med. 1976; 6:19-31.
3. Kasugai, et al., J Bone Miner Res. 2000; 15:936-943.
4. Kontoci, et al. Synth Comm. 1996;26:2037-2043.
5. Konan et al. Int. J Pharmaceutics 233, 2002, 239-252.

### Acknowledgements:

This work was funded by the Department of Defense Peer Reviewed Medical Research Program of the Office of Congressionally Directed Medical Research Programs, Contract# W81XWH-05-C-0004.

# Controlled Release of Proteasome Inhibitor from Biodegradable Nanoparticles for Myeloma Therapies

Gianny Rossini, Jack Trevino, Neal Vail  
Southwest Research Institute®, San Antonio, TX, USA, 78238  
Gianny.rossini@swri.org

## ABSTRACT SUMMARY

The objective of this study was to demonstrate nano-encapsulation and in vitro release properties of peptide aldehydes, such as MG132 and PSI, that target proteasome inhibition. The nanoparticles were composed of a mixture of two biodegradable polymers, PLGA and mPEG-PLGA at a ratio of 90:10. Encapsulation efficiency was approximately 50%, with payload varying from 0.2% for MG132 to 1.5% for PSI. A release profile was measured at 20% over a ten-day period in PBS (pH 7.5).

## INTRODUCTION

Multiple myeloma (MM) is a blood-borne disease that is uniformly fatal accounting for approximately 2% of all cancer deaths.<sup>i,ii</sup> Proteasome inhibitors are an effective therapy to prolong the life of MM patients; however, these drugs have significant side effects, such as painful neuropathy and reduced platelet and red blood cell counts. Overall, these side effects are universally seen with other chemotherapies.<sup>iii</sup>

Cancer-selective delivery systems are highly desired for chemotherapeutic agents, particularly for their ability to efficiently deliver specific drug loading to the tumor site. By confining the cytotoxic activity of the drug to within the malignant tissues, such delivery systems are envisaged to minimize indiscriminate drug distribution and lead to a focused destruction of the cancerous cells.

This research study was initiated to determine, in pre-clinical studies, the potential of skeletally targeted proteasome inhibitors as an effective and selective treatment for myeloma.

## EXPERIMENTAL METHODS

### Drug encapsulation

Encapsulation of active materials was conducted via a solvent evaporation method with minor modifications to achieve high encapsulation efficiencies.<sup>iv</sup> A 90/10 w/w mixture of PLGA and PEG-PLGA were dissolved in acetone to obtain a 1% wt. solution. Compounds were then dissolved in to this solution. The final solution was slowly injected with a needle into two volumes of 0.2% wt. sodium cholate, with continuous stirring, to produce nanoparticles. The newly formed nanoparticles were then diluted 5x into 0.1% wt. sodium cholate and stirred at room temperature for a minimum of 6 hours to evaporate the acetone. The nanoparticles were then concentrated using ultra-filtration (Millipore).

Alternatively, nanoparticles were processed with cross flow filtration (Sartorius) to remove excess solvent and to concentrate the sample volume. The final material was then lyophilized and tested for active compound by HPLC, using a Luna 2x150mm column from Phenomenex L. Samples were prepared by dissolving approximately 10mg of lyophilized nanoparticles in 100µL of DMF, brought to volume with 400µL of 30% acetonitrile, and then centrifuged at 3000 rpm. The encapsulation efficiency was calculated using the following formula:

$$EE (\%) = \frac{\text{Proteasome Inhibitor in Np (mg)}}{\text{Proteasome Inhibitor total (mg)}} \times 100\%$$

### In vitro release

An accurately-weighed quantity of nanoparticles was placed into a cellulose dialysis membrane tubing (Spectrum Laboratories Inc., CA) and immersed in 50 mL solution of 30% isopropyl alcohol. The use of a 30% isopropyl alcohol in water (as the dissolution medium) was required as a result of the poor solubility characteristics of the drug. The solution was placed in shaking incubator 4.0CFT 1570 (VWR International Int., OR) at 37 °C and 50 rpm. One milliliter of solution was withdrawn at specific time intervals. All media withdrawn was replaced with the same volume of fresh solution. The solution was analyzed by HPLC and the cumulative release calculated.

## RESULTS AND DISCUSSION

### Particle Size

Particle size (N4+, Beckman-Coulter) determination by scatter analysis was 152±12 nm (Fig. 1). Particle size remained unchanged, even after cross flow ultra-filtration system. This is important to note since ultracentrifugation procedures commonly results in particle aggregation.

SEM microphotograph supports the particle size data (Fig 2).

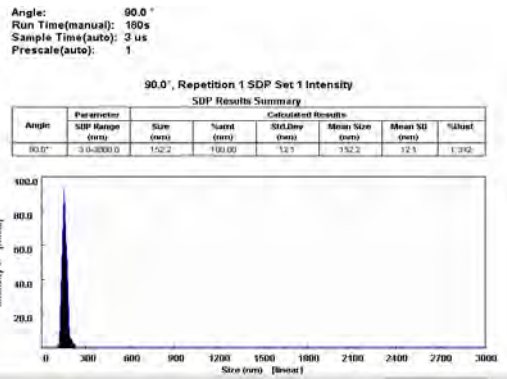


Fig 1. Nanoparticle size distribution.

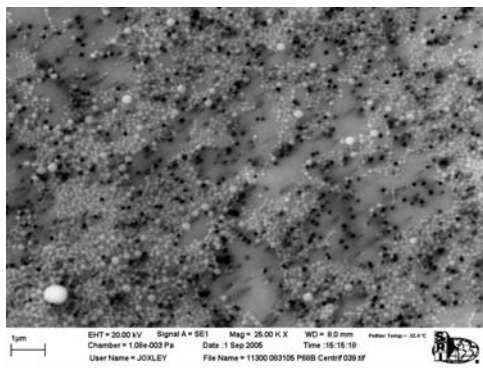


Fig 2. SEM of nanoparticles

### Drug encapsulation

Encapsulation was completed for PSI and MG132 using biodegradable polymer mixture 90/10 PLGA/mPEG-PLGA. The drug loading was 0.2% for MG132 and 1.5% w/w for PSI and the particle size was approximately 150nm±10 nm (Fig 3). The encapsulation efficiency was 50%

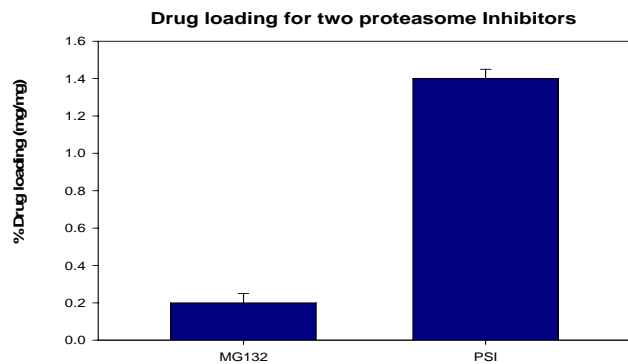


Fig 3. Drug loading for two proteasome inhibitors.

### In vitro release

It was determined that to obtain release of the active compounds at a sustainable rate, the drug loading should be limited to 1-2%. Although higher drug loadings are possible by adding compound to the nanoparticles surface, this could result in an undesirable burst release effect. In a 10 day period around 20% of loaded PSI was released. The cumulative release of PSI from two different dosages is shown in Fig. 4.

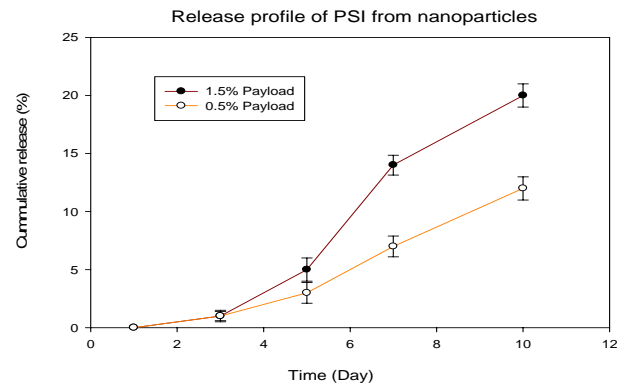


Fig 4. Drug release profile for two compositions.

Future studies includes determination of the in vitro activity using cell based assay

### CONCLUSION

Nanoencapsulation of proteasome inhibitors was achieved using a nanoprecipitation solvent evaporation protocol. No particle aggregation occurred during particle cleanup by cross flow ultra-filtration. Using a 90/10 PLGA/mPEG-PLGA we prepared particles containing up to 1.5% drug with 50% efficiency. Currently, experiments are in progress to determine the in vitro activity of the encapsulated drug using cell based assay. We will be using these results, in combination with bone-targeting nanoparticle formulations<sup>v</sup>, for future studies using in preclinical models of human multiple myeloma disease.

### REFERENCES

- <sup>i</sup> Giuliani N, Blood. 2006 Dec 15;108(13) Review
- <sup>ii</sup> Mundy G et al, Expert Opin Pharmacother. 2005 Dec;6(16):2781-91.
- <sup>iii</sup> Kropff M, Eur J Cancer. 2006 Jul;42(11):1623-39. Review
- <sup>iv</sup> Fessi H et al Pharm Res. 1998 Jul;15(7):1056-62
- <sup>v</sup> see abstract submitted to current meeting by Crumlett S

**Acknowledgement:** This work was funded by the Department of Defense Peer Reviewed Medical Research Program of the Office of Congressionally Directed Medical Research Programs.

## Development of Bone-Targeting Nanoparticles for Bone Cancer Therapies

Stefanie Crumlett, Gianni Rossini, M.S., Jack Trevino, Neal K. Vail, Ph.D.

Southwest Research Institute, San Antonio, Texas.

**Statement of Purpose.** We hypothesize that bone-targeting nanocarriers can preferentially accumulate in the skeleton and locally release proteasome inhibitors (PI) to impair the capacity of myeloma cells to survive and grow in vivo, thereby reducing the formation and growth of tumor-induced lytic bone lesions. PIs are not selective to bone and their therapeutic-toxic window may be narrow when administered systemically. Targeted bone delivery has potential to reduce systemic exposure, increase efficacy in the bone environment, and the opportunity to reverse catastrophic disease processes. Site-specific targeting requires quantitatively distinct receptors. We selected the calcified matrix as our initial site for bone-targeting. We identified bone-binding ligands and selected two well-known for their predilection to bone surfaces, methylene bisphosphonate (MBP)[1] and an aspartic acid oligopeptide (Asp<sub>n</sub>)[2]. We present work on the development and characterization of bone-targeting nanoparticles to be used in our preclinical studies.

**Methods.** Polylactide-co-glycolide (PLGA, 75/25, Brookwood) was used to prepare nanoparticles. Functional polyethylene glycols (PEG) were obtained from NOF Corp. Asp<sub>4</sub> was obtained from Sigma. PLGA-b-PEG was prepared by conjugating PLGA to an amine-terminated mPEG via DCC/NHS coupling. Maleimide-terminated PEG-b-PLA copolymer was prepared by ring-opening polymerization of lactide on to a hydroxyl-terminated bifunctional PEG. Maleimide was added to the PEG terminus by reaction with 3-maleimidopropionic acid NHS ester. Amino-MBP was synthesized by modified reported method [3]. Either aMBP or Asp<sub>n</sub> was linked via sulfhydryl-amino conversion to the functionalized copolymer. Ligand conjugation was monitored by sulfhydryl. All structures were confirmed by <sup>1</sup>H-NMR. Nanoparticles were prepared by either emulsification/solvent-loss or nanoprecipitation. Solvent was removed by evaporation. Particles were purified by ultracentrifugation or cross-flow filtration and lyophilized. Various lyoprotectants were studied. Particle size was determined by photon correlation spectroscopy and zeta-potential measured at pH 7.4. Preferential binding of ligand-containing nanoparticles to hydroxyapatite substrates was determined using radiolabeled nanoparticles. Model PIs were encapsulated and their release profiles determined in vitro.

**Results/Discussion.** In previous work, we prepared ligand-containing liposomes and showed these nanocapsules preferentially adhered to hydroxyapatite substrates in vitro [4]. However, encapsulating hydrophobic actives in liposomes is problematic. Therefore, we turned to polymer nanoparticles as an alternative. Nanoparticles were prepared from PLGA/PLA-PEG blends. Nanoparticles prepared by emulsification ranged in size from 150nm to about

200nm, depending on the PEG content, with particle size decreasing with increasing PEG content. Similarly, zeta-potential decreased with increasing PEG content, suggesting shielding of the PLGA surface by the surface PEG groups, although nanoparticle dispersion stability was not affected. Nanoparticles prepared by nanoprecipitation ranged in size from about 75nm to about 150nm, depending on solvent choice, polymer concentration, and PEG content. Lyophilization of nanoparticle dispersions resulted in irreversible agglomeration. Traditional lyoprotectants, such as oligosaccharides, reduced agglomeration, but only at concentrations of 0.5% or higher. Pluronic F68 provided excellent lyostability at considerably lower concentrations.

Structural analysis of the custom synthesized maleimide-PEG-b-PLA polymer indicated the PLA segment had a length of about 710 units, or a M<sub>w</sub> of about 50k. Attachment of the maleimide group had a conversion of 100% and ligand attachment to the maleimide was similarly determined to occur with high conversion. Ligated polymers were incorporated into PLGA nanoparticles during preparation in compositions up to about 10% wt. The gamma emitter, <sup>99m</sup>Tc, was encapsulated into nanoparticles with efficiency typically of about 20% for radiolabeling. The preferential adherence of these ligand-containing, radiolabeled nanoparticles was evaluated with several hydroxyapatite powders. Attachment of ligand-containing nanoparticles was found to occur in a Langmuir-like behavior. Nanoparticles without targeting ligands had no significant affinity for the HAP substrates.

Proteasome inhibitors PS-1, PS-IX, and MG262 were encapsulated into nanoparticle formulations with encapsulation efficiencies up to about 50%, resulting in payload compositions of typically less than about 10% wt. Particles and payload remained stable through lyoprotection. In vitro release studies showed the actives to be completely released within 1 – 3 weeks.

**Conclusions.** We prepared and verified the structure of bone-targeting ligands conjugated to biodegradable polymers and their use in the formation of polymer nanoparticles. These nanoparticles could be made lyostable with Pluronic F68 being effective at lower, reasonable concentrations than oligosaccharides. We further showed that specifically formulated bone-targeting nanoparticles preferentially adhere to bone-like surfaces. Cancer drugs could be encapsulated in these nanoparticles with reasonable efficiencies and payloads, and further released under in vitro conditions.

**References.** 1. Davis, et al., *Semin Nucl Med.* 1976; 6:19-31. 2. Kasugai, et al., *J Bone Miner Res.* 2000; 15:936-943. 3. Kontoci, et al. *Synth Comm.* 1996;26:2037-2043. 4. Vail, et al., CRS, 2003.